# DESIGN OF A SWITCHED–RELUCTANCE MOTOR DRIVE FOR ELECTRIC PROPULSION

Grant No. N00014-98-1-0617
Research Project 98PR05665 – 00
Period of Performance: May 01, 1998 – April 30, 2001

---

## Second Annual Report – Part 1 (AR2.1)

## Modeling Switched Reluctance Motors Under Multi-Phase Excitation

Roberto M. Schupbach, Shyam S. Ramamurthy, Juan Carlos Balda

University of Arkansas
Department of Electrical Engineering
3217 Bell Engineering Center
Fayetteville, AR 72701 – 1201
(501) 575-3005

Prepared for

Office of Naval Research
Ballston Center Tower One
800 North Quincy Street
Arlington, VA 22217-5660

Program Officer: Mr. Terry Ericsen



June 2000

# MODELING SWITCHED RELUCTANCE MOTORS UNDER MULTI-PHASE EXCITATION

## INTRODUCTION

The Second Annual Report has been divided into three parts in order to summarize the activities performed on this ONR grant from May 1, 1999, until May 31, 2000. The three parts are the following:

- Part 1 entitled "Modeling Switched Reluctance Motors under Multi-Phase Excitation" covers "modeling" activities performed under Task (b) - "Design of the SRM" – of this ONR Grant.
- Part 2 entitled "An Enhanced Simple Method for Designing Switched Reluctance Motors under Multi-Phase Excitation" covers "design" activities performed under Task (b) - "Design of the SRM" – of this ONR Grant.
- Part 3 entitled "Modeling Switched Reluctance Motors under Multi-Phase Excitation" covers "control" activities performed under Task (c) - "Design of the SRM Converter" – of this ONR Grant.

The reminder of this report refers to Part 1 of the Second Annual Report. This Part 1 has been divided into the following sections:

- Section A evaluates different modeling techniques available for Switched Reluctance Motors (SRM) operating under single-phase excitation.
- Section B analyzes two specific techniques for single-phase excitation; namely, the gage curve and 'look-up-table' modeling techniques.
- Section C addresses two specific techniques for multi-phase excitation of SRM; one technique is based on the 'look-up-table' used for single-phase excitation and the other implements an Artificial Neural Network (ANN) to predict the flux linkage and electromagnetic torque.

# A MODELING TECHNIQUES FOR SINGLE-PHASE-EXCITED SRM

## A.1 Introduction

Simulation must be incorporated as an integral part of the design procedure of a SRM since there are no general models or equations describing the SRM dynamic behavior. Moreover, SRM does not have the 'steady-state' operation found in traditional electric machines. The state variables (i.e. phase currents and fluxes) never reach their constant values since its principle of operation is based on a series of 'strokes'.

In the design of traditional electric machines, static and dynamic simulations have been executed as separated tasks usually performed by different engineers. In the case of the SRM, however, both types of simulation should be combined together since the SRM drive (motor/converter combination) has to be optimized for a particular application (torque vs. speed characteristic) to achieve high-performance operation [A.1].

The SRM optimization procedure is an iterative process among mathematical expressions, static and dynamic simulations as shown in Figure A-1. Therefore, it is desirable to use a Computer-Aided Design (CAD) tool to evaluate the behavior of different design parameters obtained from design equations and FEA simulation as well as different converter topologies and control strategies. This CAD tool has to predict with high accuracy the relevant performance parameters such as the time waveforms of flux linkage $\lambda(t)$, phase current $i(t)$, rotor speed $\omega(t)$, rotor position $\theta(t)$ and torque $T(t)$, from a reduced and representative group of known data or measurements. Furthermore, the selected CAD tool should be computationally efficient to reduce the time required for the optimization process.

This Section introduces the basic nomenclature and mathematical description of the single-phase excited SRM. Next, it presents and classifies different dynamic simulation techniques. Finally, it suggests the SRM modeling technique and simulation package based on the simulation goals.

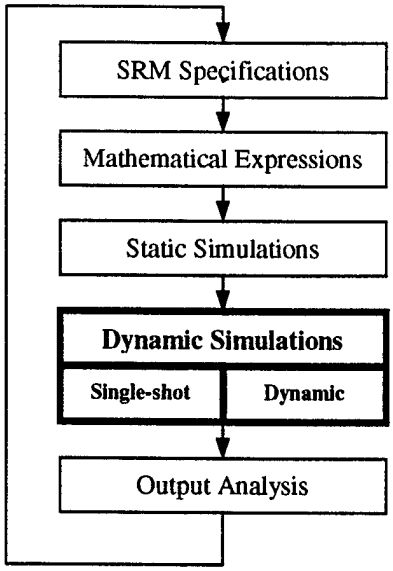


*Figure A-1 SRM optimization process.*

## A.2 Mathematical Description of the Single-Phase Excited SRM

Figure A-2 shows the basic electromagnetic structure for a 6/4 SRM. Each stator pole has a coil wound; coils are connected in such way that their magnetic fluxes are added to form a phase of the SRM. Usually, coils of opposite poles are connected in series to form a phase as shown in Figure A-2. A phase is at the *aligned position* when any pair of rotor poles is exactly aligned with respect to the excited stator poles (Phase 1 in Figure A-2). At alignment, the magnetic reluctance is at its minimum saturating the flux path at lower current levels; therefore, the inductance is at its maximum. A phase is at the *unaligned position* when the interpolar axis of any pair of rotor poles is exactly aligned with a line located at midway between two adjacent stator poles (Phase 2 in Figure A-2). It is noted that the inductance value of a phase varies widely as a function of both rotor position and phase current.

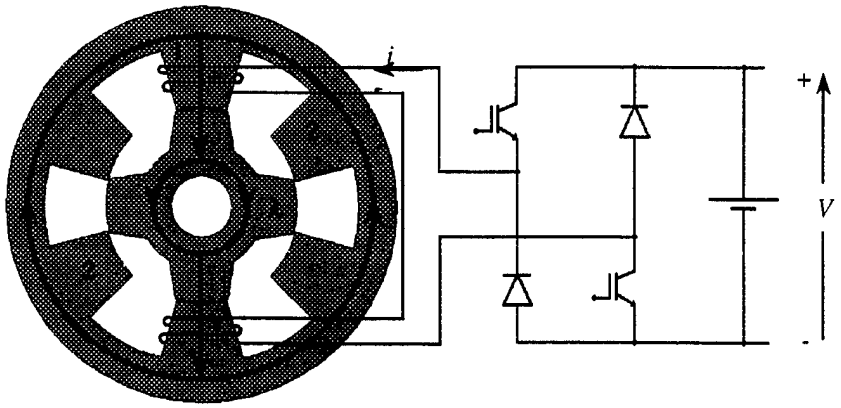


*Figure A-2 Basic SRM electromagnetic structure.*

The SRM works in a sequence of 'strokes' where the angle is given by the following equation:

$$\theta_{ST} = \frac{360^{o}}{mN_R} \tag{A-1}$$

where $m$ is the number of phases and $N_R$ is the number of rotor poles.

Typically, the number of stator poles exceeds the number of rotor poles. The torque-production capability of one rotor pole is given by

$$\beta = \frac{360^{o}}{N_R} \tag{A-2}$$

The torque capability angle is divided into two regions. In the first region, the SRM has positive torque production ($\beta_M$ motoring torque). In the second region, the SRM has negative torque production ($\beta_G$ generating torque). This is illustrated on Figure A-3. In the case of a 6/4 SRM, $\beta = 90^{o}$. Therefore, in the first 45° ($-45° \leq \beta_M \leq 0°$) the SRM develops a positive torque, and in the second 45° ($0° \leq \beta_G \leq 45°$) the SRM develops a negative torque.

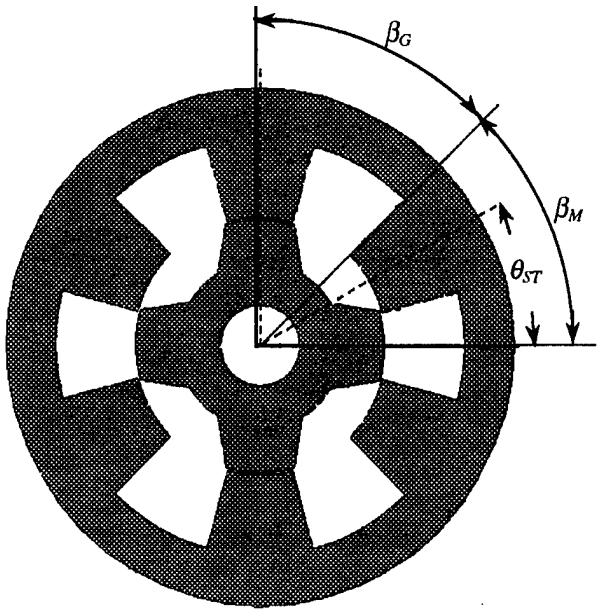


*Figure A-3 Stroke angle and torque capability angle for a 6/4 SRM.*

The SRM works under single-phase excitation if each stator pole is excited within the stroke angle. However, normally, $\beta_M = > \theta_{ST}$ given room for multi-phase excitation. If the stator pole is excited an angle larger than the stroke angle, the SRM works under multi-phase excitation. In the case of the 6/4 SRM presented in Figure A-3, $\theta_{ST} = 30°$, $\beta = 90°$ and $\beta_M = 45°$; therefore, two phases can be excited during 15° and thus developing positive torque.

If current is applied to a phase when the rotor is not at the aligned position, the rotor will be attracted to the aligned position developing a torque ideally proportional to the square of the phase current and the inductance rate of change with respect to rotor position. The most general expression for the torque produced by one phase at any rotor position is given by:

$$T(i,\theta) = \left.\frac{\partial W'}{\partial \theta}\right|_{i=const.} \tag{A-3}$$

where $W'$ is the *coenergy*, $i$ is the phase current, and $\theta$ is the rotor position. At any position, the coenergy is the area below the magnetization curve $\lambda(i,\theta)$ as shown in Figure A-4. Consequently, the coenergy is expressed as:

$$W'(i,\theta) = \left.\int_0^i \lambda(\theta,i)\, di\right|_{\theta=const} \tag{A-4}$$

where $\lambda$ is the flux-linkage.

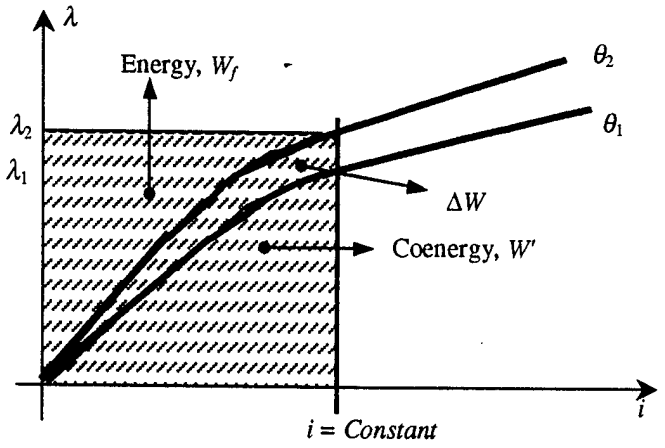


*A-4 Instantaneous torque as the rate of change of coenergy at a constant current.*

During the rotor displacement $\Delta\theta = \theta_2 - \theta_1$, there is an exchange of energy, $\Delta W$, between the supplied energy and the stored field energy. To insure that the mechanical work done is equal to the change in coenergy, constant current is assumed as the rotor moves through $\Delta\theta$. The torque can be thought as the work $\Delta W$ divided by rotor displacement $\Delta\theta$. Finally, it must be noted that

$$\omega = \frac{d\theta(t)}{dt} \tag{2-5}$$

where $\omega$ is the SRM rotor speed.

## A.3 Classification of Different Modeling Techniques

Most SRM, even those ones operating under single-phase excitation such as the 6/4 SRM, operate under multi-phase conditions for small periods of time. An accurate SRM modeling technique should take into account multi-phase operation. However, single-phase excitation modeling techniques are still being used due to several reasons:

- Single-phase modeling techniques are simpler and faster than multi-phase excitation modeling techniques.
- The number of data points required for multi-phase modeling technique increases exponentially with the number of excited phases.
- Multi-phase operation can be modeled as a superposition of several single-phases assuming linearity.

It is not the case of the SRM since it works under high magnetic saturation; therefore, its description is non-linear. However, this type of approximation frequently provides enough accuracy as a first approach to model the SRM dynamic behavior or the control technique. For higher modeling accuracy, specific multi-phase excitation modeling techniques are required.

Most of the simulation techniques use a curve-fitting technique to represent the flux-linkage surface. Such a technique requires a large number of measured or calculated data points. Figure A-5 shows the flux-linkage characteristic of a 6/4 SRM calculated using FEA simulations. The FEA of a SRM is a complex and time-consuming but unavoidable task in the design of high-performance SRM drives. The code writing and debugging (setup time) of a FEA simulation takes approximately a week (40 hours). A single simulation point in a SUN® workstation machine (100 MHz clock CPU and 120 Mbits RAM) takes approximately 4 minutes.

Figure A-5 has 225 points (15 different rotor positions times 15 different current levels). Consequently, once that the FEA code is debugged, it takes approximately 15 hours to finish the complete flux-linkage 'mapping' of a 6/4 SRM. If a two-phase excitation is assumed, the number of required FEA points in order to have the same accuracy will be 3375 (15 different rotor positions times 15 different $i_1$ levels times 15 different $i_2$ levels) requiring 225 hours of simulation (approximately 10 days, 24 hours a day) and a large amount of storage space. Therefore, a different approach is required for multi-phase modeling of the SRM to reduce the number of needed data points.

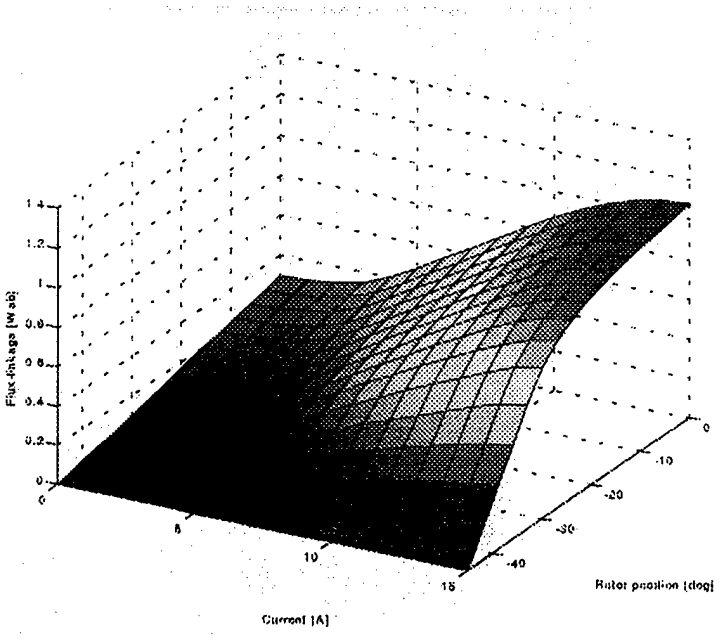


*Figure A-5 The 6/4 SRM flux-linkage characteristic $\lambda(\theta,i)$.*

The modeling of a single-phase excited SRM is based on the torque equation (i.e., (A-3) and (A-4)), and the voltage equation of the stator phase, which is expressed as:

$$\pm V(t) = Ri(t) + \frac{d\lambda(\theta(t), i(t))}{dt} \tag{A-6}$$

where $V$ is the voltage applied to a phase and $R$ is the phase resistance.

Several characteristics can be used to classify single-phase excited SRM modeling techniques. Here, the approach solving (A-6) is utilized as a classification parameter. As Figure A-6 illustrates, three different categories are determined, namely: the *flux-linkage* approach, the *inductance* approach, and the *phase-current* approach.

From Figure A-6, it is noted that the flux-linkage approach is based on one of the most general solutions of (A-6) which is the calculation of a flux-linkage equation $\lambda(\theta(t), i(t))$ to be derived with respect to time. This approach is simple; however, it is very sensitive to measurements or calculations errors of the data points since the solution is based on the derivative of a function obtained through curve-fitting techniques.

A different solution is adopted on the inductance approach where equations for the derivative of the flux linkage with respect to rotor position (back-EMF) and derivative of the flux linkage with respect to current (inductance) are obtained. This solution avoids the sensitivity problem of the previous solution; however, it requires solving two equations instead one.

Finally, in the phase-current approach the flux linkage is obtained through integration requiring an expression for the phase current $i(\theta(t), \lambda(t))$ as shown in Figure A-6. This approach avoids the sensitivity problem of the first approach and presents a simpler solution than the second approach.

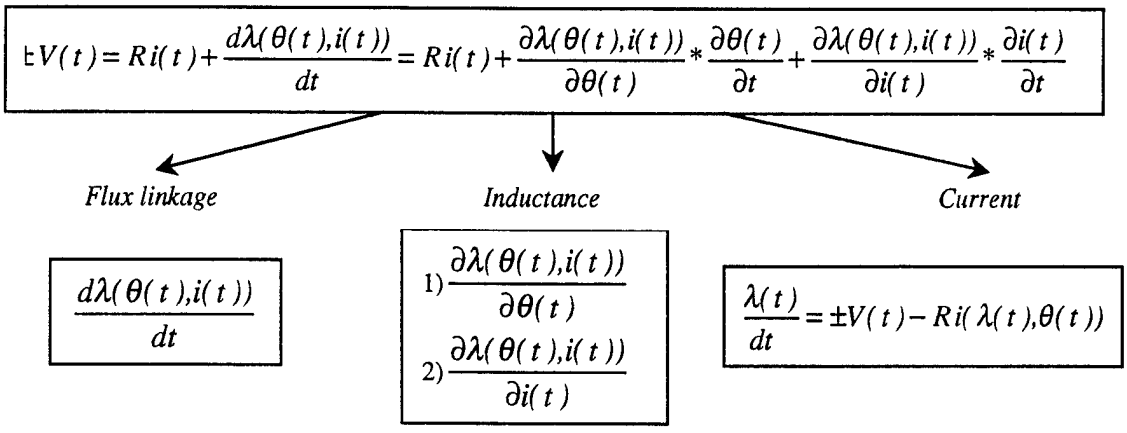


*Figure A-6 Classification of modeling techniques for single-phase excited SRM.*

In the next three sub-sections, the three approaches (flux-linkage, inductance and phase-current) are explored presenting an historical evolution of each approach, a description of the different used curve-fitting techniques and the data requirements.

### A.3.1 The flux-linkage approach

A mathematical expression for the flux linkage $\lambda(\theta(t),i(t))$ is first obtained using different curve-fitting techniques. Next, the derivative with respect to time of the flux linkage $\frac{d\lambda(\theta(t),i(t))}{dt}$ is obtained in order to solve (A-6).

Several curve-fitting techniques or combination of these have been used to approximate the flux linkage $\lambda(\theta(t),i(t))$, namely: Fourier series, exponential series, polynomial, etc. Several approaches were summarized by Fulton and Stephenson in [A.1]. Here, the two principal techniques are considered; namely

- Polynomial and Fourier series approximations.
- Sum of exponential approximations.

#### *A.3.1.1 Polynomial and Fourier series approximations*

Pickup and Tipping presented one of the first descriptions of the flux linkage $\lambda(\theta,i)$ using polynomial approximations [A.2]. In this work, both the rotor position and phase current are approximated by a sum of exponential functions. In a latter method, a Fourier series is used to approximate the flux linkage $\lambda(\theta,i)$ as a function of the rotor position, and a polynomial approximation to describe the flux linkage $\lambda(\theta,i)$ as a function of the phase current. Analytical expressions for $\frac{\partial\lambda}{\partial\theta}(\theta,i)$, $\frac{\partial\lambda}{\partial i}(\theta,i)$ and $T(\theta,i)=\frac{\partial}{\partial\theta}\left\{\int_0^i\lambda(\theta,i)di\right\}$ are determined from the obtained analytical expression for $\lambda(\theta,i)$. However, the time-consuming process of obtaining the complete description of the flux linkage vs. current with respect to rotor position is required to obtain the coefficients of these analytical expressions. This 'mapping' process consists on the measuring/calculation of the flux linkage ($z$-axes) at $x$-degree rotor-position intervals and $y$-A winding-current intervals (see Figure A-5).

#### *A.3.1.2 Sum of exponential approximations*

This approach is presented by Ilic-Spomg *et. al* in [A.3]. Lately, Byne and Dwyer presented in [A.4] a simplified version of the same approach. In this work, the sum of three exponential functions is used to fit the curve $\lambda(\theta,i)|_{\theta=cte}$ using the flux linkage measured at equally-spaced rotor positions and phase currents.

$$\lambda(\theta,i)=a_1(\theta)\left[1-e^{a_2(\theta)i}\right]+a_3(\theta)i$$

where $a_x(\theta)=\sum_{k=0}^{n} A_{xk}\cos(\alpha\theta)$; $x$ = *1,2,3*. Analytical expressions for $\left.\frac{\partial\lambda}{\partial i}(\theta,i)\right|_{\theta=const}$ and $\left.\int_0^i \lambda(\theta,i)di\right|_{\theta=const}$ are determined, and values of $\left.\frac{\partial\lambda}{\partial\theta}(\theta,i)\right|_{\theta=const}$ and $T(\theta,i)=\frac{\partial}{\partial\theta}\left\{\int_0^i \lambda(\theta,i)di\right\}$ are subsequently calculated. Any intermediate value of $\left.\frac{\partial\lambda}{\partial i}(\theta,i)\right|_{\theta=const}$, $\left.\frac{\partial\lambda}{\partial\theta}(\theta,i)\right|_{i=const.}$ and $T(\theta,i)$ are determined by means of linear interpolation. However, the complete description of the flux linkage vs. current with respect to rotor position is required as in *A.3.1.1*.

The exponential-sum concept with some slightly modifications is used by Torrey *et. al* in different publications. In [A.5], the exponential-sum concept is incorporated in the simulation of a 60 kW SRM. However, once again, the complete description of the flux linkage vs. current with respect to rotor position is required to obtain the coefficients of the exponential functions. In addition, the SRM is only simulated at constant speed. In a later publication [A.6], relations between the coefficients of the exponential sum and the physical structure of the SRM are presented. The goal of that work is the reduction of the number of measured data or the need for FEA simulations. However, an iterative analysis is required to obtain certain parameters. Moreover, there are differences between measured and predicted waveforms.

In summary, the latest version of the flux-linkage approach reduces successfully the number of required data points; however, the sensitivity of this method to measurements or calculations of the data point errors is still present. In order to eliminate this sensitivity problem, curve-fitting techniques are used to approximate the two partial derivatives of the flux linkage in the inductance approach.

### A.3.2 The inductance approach

The two partial derivatives of the flux linkage, the inductance $\left.\frac{\partial\lambda}{\partial i}(\theta,i)\right|_{\theta=const}$ and the 'back-EMF' $\left.\frac{\partial\lambda}{\partial\theta}(\theta,i)\right|_{i=const.}$ are obtained using approximation techniques. Mahdave *et al.* presented in [A.7] a method based in the same principle used by Pickup and Tipping in [A.2]. In this method, a Fourier series as a function of rotor position and a polynomial approximation as a function of phase current are used to approximate the inductance and the back-EMF, respectively. The coefficients of the Fourier series are obtained from a relation among the values of the inductance at three different rotor positions: aligned, unaligned and midway. The coefficients of the polynomial approximation used to represent the relationship between phase inductance and the back-EMF are derived using few data points from FEA or measurements. Therefore, the complete description of the flux linkage vs. current with respect to rotor position is not required. Finally, an analytical expression for torque $T(\theta,i)$ is determined using the inductance and back-EMF analytical expressions.

The principal contribution of this approach is the elimination of the data-error sensitivity problem of the flux-linkage approach. In addition, the amount of data required from FEA

simulations or measurements is reduced. However, this approach presents a more difficult implementation and a smaller accuracy than the flux-linkage approach.

In order to combine the advantages of the flux-linkage and inductance approaches (A-3) is solved using a complete different approach which is introduced in the next section.

### A.3.3 The phase-current approach

The phase voltage equation, (A-3), is reformulated as follows:

$$\frac{d\lambda(\theta,i)}{dt} = \pm V - R * i(\theta,i) \qquad \text{(A-7)}$$

This non-linear differential equation is solved through numerical integration; instead of derivation as it was done in the two previous approaches. This improves the solution accuracy and robustness to numerical problems.

Several techniques have been used to approximate the phase current required in the integration of (A-7). Here, the three principal techniques are only considered; namely:

- Non-linear differential equation
- Piecewise low-order polynomial
- Gage curve

#### *A.3.3.1 Non-linear differential equation*

The idea of presenting (A-6) as a non-linear differential equation is initially presented by Stephenson and Corda in [A.8]. The main objective of this approach is to avoid the fundamental difficulty of obtaining accurate values for the differential of a function that is only specified by tabulated points. The solution of (A-7) is given by:

$$\lambda(\theta(t),i(t)) = \int_0^t [\pm V(t) - Ri(\theta(t),\lambda(t))]\,dt \qquad \text{(A-8)}$$

At each step of the numerical integration of (A-8), a value of $i(\lambda,\theta)$ is calculated performing a quadratic interpolation in $\lambda$, and a linear interpolation in $\theta$ from stored values.

The coenergy is calculated using numerical integration of $W'(\theta,i) = \int_0^i \lambda(\theta,i).di\big|_{\theta=const}$, and subsequently the torque $T(\theta,i) = \frac{\partial W'(\theta,i)}{\partial\theta}\Big|_{i=const}$ is determined from the expression of coenergy through numerical differentiation. This method avoids the calculation of differential

coefficients. However, the complete description of the flux linkage vs. current with respect to rotor position is required. In addition, the accuracy of the torque waveform is reduced because of the numerical differentiation.

### *A.3.3.2 Piecewise low-order polynomial*

The piecewise low-order polynomial concept is presented by Miller in [A.9]. Here, (A-7) is solved using numerical integration as in the previous method; however, instead of a set of stored values, a 'sinusoidal' interpolation is used to calculate the current value of $i(\lambda, \theta)$ required at each step of the numerical integration as shown in Figure A-7. Therefore, the complete description of the flux linkage vs. current with respect to rotor position is not required any longer. However, once again, the torque waveform is obtained through the numerical differentiation reducing its accuracy.

In order to improve the accuracy of the torque waveform, an analytical expression instead a numerical differentiation is required. The concept of the gage curve introduced in the next section allows obtaining such an analytical torque expression.

### *A.3.3.3 Gage curve*

The use of this concept in SRM applications is introduced by Miller in [A.10]. Gage curves are used to get the instantaneous current values required on the calculation of (A-5) from the known rotor position and flux linkage.

As shown in Figure A-8a, this concept is similar to the sinusoidal-interpolation concept. However, the current level is used as a parameter (instead of the flux linkage) as shown in Figure A-8b.

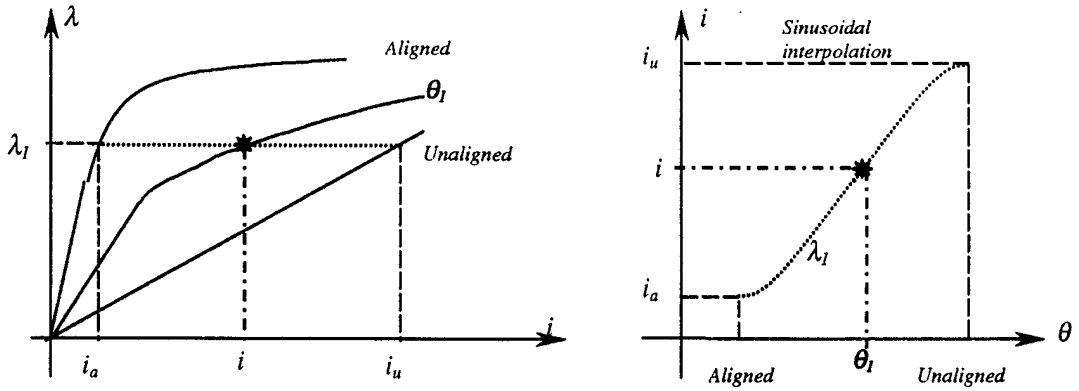


*Figure A-7a Flux-linkage λ vs. current with θ as parameter.*

*A-7b Sinusoidal interpolation for phase current i.*

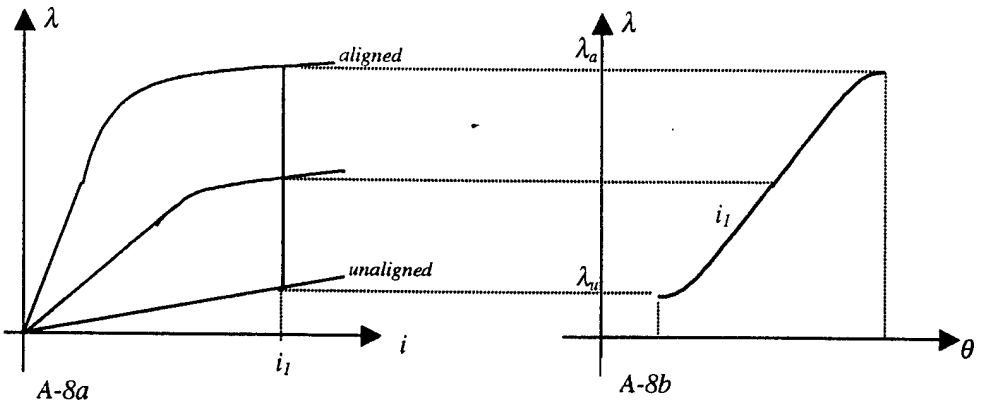


*Figure A-8a Flux-linkage λ vs. current with θ as parameter. A-8b Gage curve for different current levels.*

As in the sinusoidal-interpolation concept, mathematical expressions for the unaligned and aligned flux-linkage curves are required in order to define the gage curve. However, using the gage curve, the original flux linkage can be expressed as the product of two functions. Thus, the integration of the flux linkage (A-4) yields an explicit expression for the coenergy allowing deriving an expression for the instantaneous torque. The principal advantage of this technique is that phase current and torque are obtained from an analytical equation eliminating numerical differentiation and the need for a large number of FEA simulations. In addition, a small computational time is achieved because of the simple formulation of the gage-curve equations. The disadvantage of this method is the empirical formulation of the gage curve. Consequently, there is not a strong relation between the equations and the SRM physical parameters.

The gage-curve concept is also used in [A.11] where the set of required data is reduced, and a new method to model the unaligned and aligned flux-linkage curves is presented. Finally, an ultra-fast SRM model based on the gage-curve concept is presented in [A.12] where the gage curve is normalized to allow a simpler formulation and a smaller computational time.

Based on its numerous advantages, the gage-curve method was initially selected in this Research to model a 6/4 SRM. However, implementing the ultra-fast gage-curve modeling technique [A.12] in Matlab/Simulink requires the solution of complex mathematical expressions demanding the use of different Matlab functions; therefore, the Simulink *Matlab Function* block has to be repeatedly used. In order to perform the different calculations, the Simulink *Matlab Function* block sent the function inputs data from the Simulink workspace to the Matlab workspace where the function is executed as any Matlab function. Once it is executed, the outputs are saved on the Matlab workspace and sent back to the Simulink workspace to be the outputs of the *Matlab Function* block. This exchange of information between Simulink and Matlab workspaces has a negative impact in the simulation computational time. Moreover, time-consuming functions such as cubic-spline interpolation, polynomial fitting, or polynomial-roots solution are normally required; therefore, the computational time is further increased. A new modeling technique is introduced in the next section in order to avoid the above-mentioned disadvantages.

## A.4 Modeling Technique Based on 'Look-Up Tables'.

This modeling technique solves (A-7) through numerical integration; therefore, it classifies under the *current approach* category. However, the 'look-up tables' modeling technique is classified here under a new category since this technique will be used as comparison through this entire report.

The operation principle of this technique is very simple; (A-6) is solved through numerical integration to obtain the flux linkage as done in any phase-current approach. However, the required values of $i(\lambda, \theta)$ are now calculated using a Simulink look-up table which performs a cubic interpolation between the stored data. The flux linkage and the rotor position are required as inputs.

Another Simulink look-up table is used to obtain the instantaneous torque $T(i, \theta)$ in which the phase current and rotor position are required as inputs. Figure A-9 shows the Simulink schematic implementation of the 'look-up-table' based model.

The modeling technique based on 'look-up tables' is able to overcome almost all the disadvantages of previous methods presenting a very simple structure and implementation and high accuracy. In addition, this technique provides an excellent link between static (FEA) and dynamic simulations. Finally, all mathematical expressions are implemented using 'pure' Simulink blocks improving further the computational time.

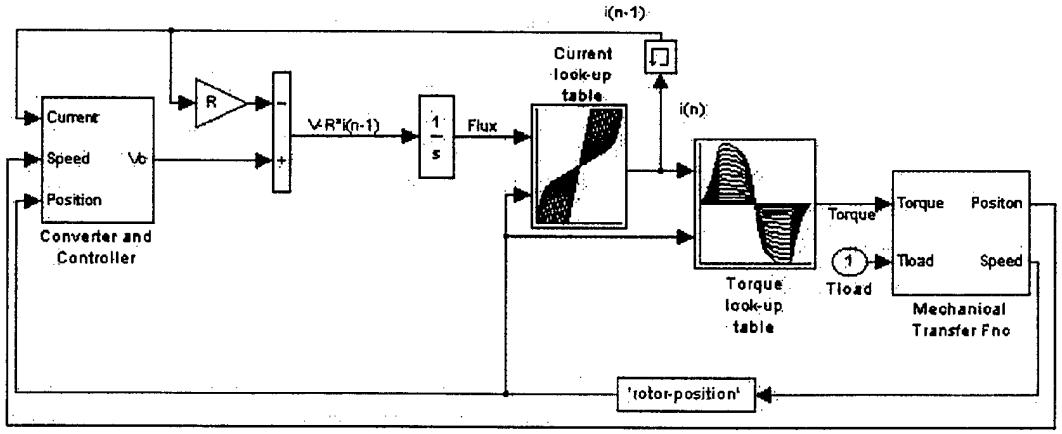


*Figure A-9 Schematic block diagram of the 'look-up table' modeling technique.*

The disadvantage of this modeling technique is that the complete description of *(a)* current vs. flux linkage with respect to rotor position, and *(b)* torque vs. current with respect to rotor position are required. Finally, note that even thought the full 'mapping' of the SRM flux linkage by means of FEA is a time-consuming process, the time required to obtain the data *(a)* using FEA is the same as the time required to obtain the data *(a)* and *(b)* since both results can be obtained at the same time. In addition, it is assumed that the SRM physical dimensions are designed using FEA results; therefore, the code required for the FEA simulation is available eliminating one of the most time-consuming parts of a FEA simulation.

## A.5 Selection of the SRM Modeling Technique

The application area and characteristics of the SRM model should be established in order to select the dynamic modeling technique. FEA-based software packages has been proving to be the most suitable type of software for SRM static simulations. FEA-based software are used for the design of the motor itself and the analysis of different SRM topologies such as short-, full- and fractional-pitch windings, multi/single-phase excitation, etc. On the other hand, circuit-based software packages such as SPICE or Saber are more suitable for the design of the converter. Using this software, different converter topologies, snubber, gate and protection circuits are studied. Finally, a SRM model capable of accurate prediction of the main SRM waveforms and a small computational-time is required in the design of the controller and control algorithm.

In a traditional SRM design procedure, a preliminary design is obtained using mathematical expressions and static FEA-based simulations. All the SRM physical dimensions as well as parameters such as static torque, number of turns, current and voltage ratings are obtained on this first step of the design procedure. If such FEA-based simulations were used, the remaining application area of the SRM model is the prediction of the dynamic behavior to develop the controller and control algorithms. Therefore, the dynamic modeling technique selected should have the following characteristics:

- Accurate prediction of $T(t)$, $\lambda(t)$, $i(t)$, $\omega(t)$, and $\theta(t)$.
- Capability of modeling different SRM topologies (6/4, 8/6, etc.) as well as different types of winding pitch; i.e., short, full and fractional.
- Capability of modeling different types of excitation; i.e., single- and multi-phase excitation.
- Small computational-time requirements to reduce the developing time of the control algorithm.
- Interaction with FEA-based software.
- Reduced setup time.
- Reduced set of parameters and data points.

- Flexibility for future modifications or additions; i.e., loss calculations.

The modeling technique based on the gage-curve concept is one of the most suitable techniques to accomplish some of the above-mentioned features. The particularly simple structure of the gage curve is the key to not only the modeling of the main non-linearities related with the variable geometry of the SRM but also to small computational-time requirements. However, the gage curves are based on empirical equations; therefore, the design of the SRM using this technique is not straight forward since the results of the simulation cannot be easily translated into the physical parameters of the SRM. In addition, the gage-curve modeling technique has a complex setup; consequently, its understanding and implementation are time consuming. Moreover, the advantage of the reduced data set required from FEA simulations is reduced by the fact that one of the most difficult steps in a FEA-based simulation is its setup (code writing and debugging). In other words, the man-hours required for the setup of a few FEA simulation points or some hundred points are almost the same.

To overcome the disadvantages presented by the gage-curve modeling technique, the 'look-up-table' modeling technique is developed and implemented in this research. Among the most outstanding advantages of this modeling technique are its extremely simple implementation and its improved computational efficiency compared with the gage-curve modeling technique. The main disadvantage is the larger number of data required from FEA simulations; however, this data is available since the SRM is assumed to be designed using FEA. Therefore, the benefits of the 'look-up-table' modeling technique outnumber its drawbacks. The last step on the selection of the SRM modeling technique is the selection of the software used to implement the two-selected modeling technique. This is done in the next section.

## A.6 Selection of the Software Implementing SRM Modeling Techniques

The software selected to implement the SRM dynamic model should allow to handle several parts of the system that are very different in nature. In general, converters are modeled using its circuit representation. Controller and control algorithms are expressed in terms of mathematical expressions such as differential or difference equations, transfer functions, etc. Mechanical loads are modeled using differential equations. Finally, mathematical tools such as the Laplace transform, interpolation, integration, differentiation will be required for the modeling of an SRM drive. Several simulations package such Saber in [A.13] and Pspice in [A.14-A.15] have been used on the implementation of the dynamic simulation technique. However, Matlab/Simulink is selected here to implement the two modeling techniques, gage curves and 'look-up' tables, because Matlab/Simulink meets all the above mentioned conditions and presents the following characteristics:

- Powerful tool for analyzing and developing the controller and control algorithms.
- Programming capability (Matlab, C) with extended libraries.
- Interface with other programs that can be used in the development of other parts of the system, such as Saber in the development of the converter.

- Large Mathematical libraries.
- Worldwide known.

Finally, other modeling techniques to be developed in the future can be easily implemented in Matlab/Simulink.

## A.7 Summary

In this Section, the basic mathematical description of a single-phase excited SRM and the difficulty of an accurate modeling of the SRM were firstly presented introducing the need of an integrated CAD tool in the design of a SRM drive. Next, a classification of different modeling approaches was performed. Table A-1 summarizes the advantages and disadvantages of the modeling approaches reviewed in this Section. Two modeling techniques, the 'gage-curve' and 'look-up-tables', were selected to be implemented in Section B. Finally, Matlab/Simulink was selected as the software package to be used in the implementation of the selected simulation techniques.

*Table A-1 Advantages and disadvantages of different SRM modeling techniques.*

| Modeling Technique | Advantages | Disadvantages |
|---|---|---|
| **Flux Linkage**<br>Polynomial and Fourier series approximation<br>Sum of exponential approximation | Simplicity | Large number of input data<br>Limited accuracy because of numerical differentiation<br>Large computational-time requirements |
| **Inductance** | Reduced number of input data<br>Elimination of numerical differentiation | Complex mathematical description<br>Limited accuracy because of pour behavior of the curve fitting |
| **Phase Current**<br>Non-linear differential equation<br>Piecewise low-order polynomial | Elimination of numerical differentiation | Large computational-time requirements because of computing the integral of coenergy |
| Gage curve | Small computational-time requirements<br>Small number of input data | Complex mathematical description and understanding<br>Long setup time<br>Empirical method<br>Limited accuracy |
| Look-up table | Simplicity<br>Accuracy<br>Very small computational-time requirements<br>Very small setup time | Large number of input data |

## A.8 References


[A.1] N.N. Fulton, J.M. Stephenson, "A Review of Switched Reluctance Machine Design", *International Conference on Electric Machine*, 1988.

[A.2] Pickup, Tipping, "Method of Predicting the Dynamic Response of a Variable Reluctance Stepping Motor", *IEE Proceeding*, Vol. 120, No. 7, 1973, pp. 757-765.

[A.3] Ilic-Spong, M. Marino, R. Peresada, D.G. Taylor, "Feedback Linearizing Control of Switched Reluctance Motors", *IEEE Transactions on Automation and Control*, 1987, pp. 371-379.

[A.4] J.V. Byrne, J.B. O'Dwyer, "Saturable Variable Reluctance Machine Simulation Using Exponential Functions", *Proceeding of the International Conference on Stepping Motors and Systems*, University of Leeds, UK, July 1976, pp. 11-16.

[A.5] D.A. Torrey, J.H. Lang, "Modeling a Non-Linear Variable-Reluctance Motor Drive", *IEE Proceeding*, Vol. 137, Pt. B, No. 5, September 1990, pp. 312-326.

[A.6] D.A. Torrey, X-M Niu, E.J. Unkauf, "Analytical Modeling of Variable-Reluctance Machine Magnetization Characteristics", *IEE Proceeding on Electronic Power applications*, Vol. 142, No. 1, January 1995, pp. 14-22.

[A.7] L. Mahdave, W. F. Ray, P. J. Lawrenson, R. M. Davis, J. M. Stephenson, N. N. Fulton, R. J. Blake, "High Performance Switched Reluctance Brushless Drives", *IEEE Industry Applications Society Annual Meeting*, 1985, New York , USA, pp. 231-237.

[A.8] J.M. Stehpenson, J. Corda, "Computation of Torque and Current in Doubly-Salient Reluctance Motors From Non-Linear Magnetization Data", *Proceedings IEE*, Vol. 126, May 1979, pp. 321-327.

[A.9] T. Miller, M. McGilp, "PC-CAD for Switched Reluctance Drive", *Electric Machine and Drive Conference*, London, December 1987, No. 282, pp. 360-366.

[A.10] T. Miller, Switched Reluctance Motor and Their Control, Manga Physics Publishing and Clarendon Press - Oxford, 1993.

[A.11] T. Miller, M. McGilp, "Non-Linear Theory of the Switched Reluctance Motor for Rapid Computer-Aided Design", *IEE Proceeding*, Vol. 137, Pt. B, No. 6, November 1990, pp. 337-347.

[A.12] T. Miller, M. Glinka, M. McGilp, C. Cossar, G. Gallegos-Lopez, D. Ionel, M. Olaaru, "Ultra-Fast Model of the Switched Reluctance Motor", *Proceeding of the Industrial Applications Society Annual Meeting*, 1998, pp. 319-326.

[A.13] D.A. Torrey, "An Experimentally Verified Variable-Reluctance Machine Model Implemented in the Saber™ Circuit Simulator ", *Electric Machines and Power Systems*, Vol. 24, No 2, 1996, Taylor & Francis Ltd., pp. 199-209.

[A.14] G. Franceschini, S. Pinari, M. Rinaldi, C. Tassoni "Spice-Assisted Simulation of Controlled Electrical Drives: An Application to Switched Reluctance Drive", *IEEE Transactions on Industry Applications*, Vol. 27, No. 6, November-December 1991, pp. 1103-1110.

[A.15] J. Mahadavi, G Sureseh, B. Fahimi, M. Ehsani, "Dynamic Modeling of Non-Linear SRM Drive With PSPICE ", *IEEE Transactions on Industry Applications Society Annual Meeting*, New Orleans, Louisiana, October 5-9, 1997, pp. 661-667.

# B IMPLEMENTATION OF MODELING TECHNIQUES FOR SINGLE-PHASE-EXCITED SRM

## B.1 Introduction

Several modeling techniques predicting the dynamic behavior of a single-phase-excited SRM were introduced in Section A. Each modeling technique has different application areas, accuracy, computational-time requirements and ability to model non-linearities associated with the SRM structure. Two different modeling techniques were selected; namely, the 'gage-curve' and 'look-up-table' modeling techniques.

The modeling technique based on the gage-curve concept was selected because of its right balance among data requirements, computational-time requirements, and accuracy on the prediction of the principal waveforms (flux linkage, phase current, torque, etc).

The modeling technique based on the 'look-up tables' concept was selected because it presents a very simple structure, small computational time, and high accuracy on the prediction of the principal waveforms. In addition, this modeling technique provides an excellent link between static (FEA) and dynamic simulation results as it will be shown in this Section.

## B.2 The Gage-Curve Modeling Technique

The fundamental relationships among flux linkage, phase current and rotor position are given by the magnetization curves as shown in Figure B-1a. The gage curves can be seemed as a graphical transformation of the classical magnetization curve. The gage curves are plotted as flux linkage vs. rotor position with current as parameter; its representation lies in a normal plane with respect to the magnetization curve plane [B.1]. Using this new representation, the original flux linkage can be expressed as the product of two functions, $\lambda(i,\theta) = f1(i)\ f2(\theta)$ which can be incorporated into (A-4) to be integrated. Therefore, it is not necessary to evaluate the integral of the coenergy (A-4) at every time step of the simulation process since an explicit expression for the instantaneous torque can be derived from the coenergy expression [B.2].

As shown in Figure B-1b, the gage curve changes its size and shape with phase current level (or saturation level). Thus, the gage curve should model accurately these changes in shape and remain as mathematically simple as possible; this is the essential requirement for a small computational time.

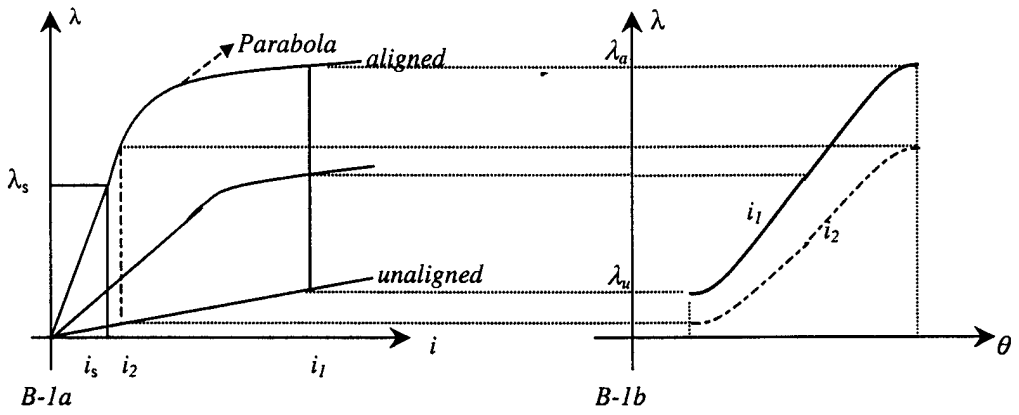


*Figure B-1a Flux linkage λ vs. phase current i with rotor position θ as parameter. B-1b Gage curve for two different phase current levels.*

### B.2.1 Incorporation of the Gage-Curve Concept Into Dynamic Simulations

In the gage-curve modeling technique, (B-3) that is repeated here for convenience as (B-1),

$$\pm V = Ri + \frac{d\lambda(\theta,i)}{dt} \tag{B-1}$$

is solved through numerical integration in order to obtain

$$\lambda(\theta,i) = \int_0^t [\pm V - Ri(\theta,\lambda)]dt \tag{B-2}$$

where $V$ is the applied phase voltage, $i$ is the phase current, $\lambda$ is the flux linkage and $\theta$ is the rotor position.

The phase-current value that is required at each time step on the numerical solution of (B-2) is determined from the gage curve using 'past' values of the flux linkage and rotor position. In addition, mathematical expressions are derived to calculate the instantaneous torque. Finally, speed and position are calculated using the following mechanical equations:

$$T_e(t) - T_L(t) = J_T \frac{d^2\theta}{dt^2} + B_T \frac{d\theta}{dt} \tag{B-3}$$

$$\theta = \int_0^t \omega \, dt + \theta_0 \tag{B-4}$$

where $T_L$ is the load torque, $J_T$ is the total inertia of the system, $B_T$ is the total friction coefficient, $\omega$ is the instantaneous SRM rotor speed, and $\theta_0$ is an arbitrary initial rotor position.

### B.2.2 Mathematical Formulation of the Gage Curve

As shown in Figure B-1b, gage curves change in size and shape with phase current level. The gage curves are normalized in order to be independent of size changes and simplify the mathematical definition and solution of the equations. This normalization is made in such a way that if there were no magnetic saturation, there would be only one normalized curve for all current levels [B.3]; meaning that the gage curve would be, in addition, independent of shape changes. Unfortunately, SRM works under deep saturation, requiring that the normalized gage curve models those shapes changes accurately in order to maintain the accuracy of the modeling technique.

The flux linkage, $\lambda$, is normalized as follows:

$$y(x) = \frac{\lambda(x) - \lambda_u}{\lambda_a - \lambda_u} \tag{B-5}$$

where $y(x)$ is the normalized flux linkage, $\lambda_a$ is the flux linkage at the aligned rotor position, $\lambda_u$ is the flux linkage at the unaligned rotor position, and $\lambda(x)$ is the flux linkage at any intermediate rotor position.

The rotor position, $\theta$, is normalized as follows:

$$x = \frac{\theta - \theta_u}{\theta_a - \theta_u} \tag{B-6}$$

where $\theta_a$ is the aligned rotor position, $\theta_u$ is the unaligned rotor position, and $\theta$ is any intermediate rotor position.

The normalized gage curve is divided into five subintervals in order to define representative mathematical expressions for $y(x)$ in each subinterval as shown in Figure B-2. The points J and K are determined by the pole arc; J is the point in which the stator and rotor poles start to overlap, and K is the point in which the stator and rotor poles are completely overlapped [B-4]. Note that this report follows the notation used by Miller on [B-4].

Region *d* extends from the point U to $x = J_0 = xJ0$ where $y(x)$ is defined as:

$$y(x) = 0$$

Region *e* extends from $x = K_1 = xK1$ to point A where $y(x)$ is defined as:

$$y(x) = 1$$

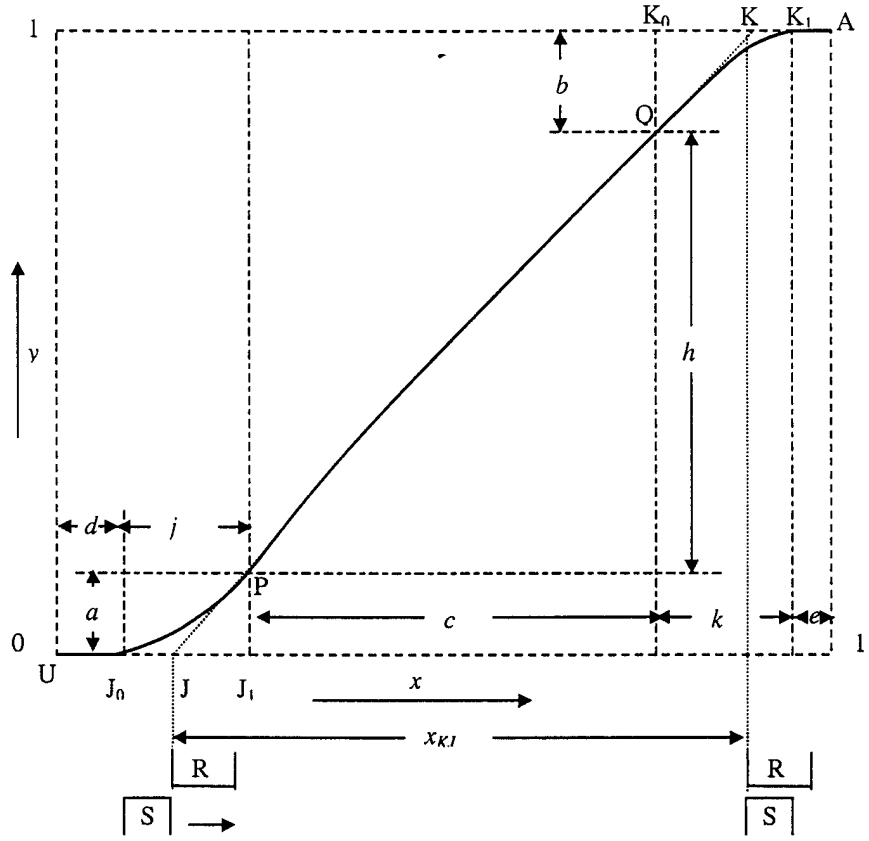


*Figure B-2. Normalized gage curve.*

Region *j* extends from $x = J0 = x_{J0}$ to $x = J_1 = x_{J1}$ where $y(x)$ is defined as:

$$y(x) = \frac{m_P}{2}\left[u - \frac{\sin(qu)}{q}\right] \tag{B-7}$$

where $u = x\text{-}x_{J0}$ and $q = \pi/j$. In this region, the first and second derivatives of the normalized flux linkage are given by:

$$\frac{dy}{dx} = \frac{du}{dx} = \frac{m_P}{2}[1 - \cos(qu)] \tag{B-8}$$

$$\frac{d^2y}{dx^2} = \frac{m_P}{2} q \sin(qu) \tag{B-9}$$

Equation (B-8) ensures that there is no discontinuity in the rate of change of $y(x)$ when moving to the adjacent regions $d$ and $c$ since $\left.\frac{dy}{dx}\right|_{x=x_{J_0}} = 0$ and $\left.\frac{dy}{dx}\right|_{x=x_{J1}} = m_p$, respectively.

Region $k$ extends form $x = K_0 = x_{K0}$ to $x = K_1 = x_{K1}$ where $y(x)$ is defined as:

$$y(x) = 1 - \frac{2k}{\pi} m_Q [1 - \sin(rz)] \tag{B-10}$$

where $z = x - x_{K0}$ and $r = \pi/2k$. In this region, the first and second derivatives of the normalized flux linkage are given by:

$$\frac{dy}{dx} = \frac{dy}{dz} = m_Q \cos(rz) \tag{B-11}$$

$$\frac{d^2y}{dx^2} = -m_Q r \sin(rz) \tag{B-12}$$

Equation (B-11) ensures that there is no discontinuity in the rate of change of $y(x)$ when moving to the adjacent regions $c$ and $e$ since $\left.\frac{dy}{dx}\right|_{x=x_{K_0}} = m_Q$ and $\left.\frac{dy}{dx}\right|_{x=x_{K1}} = 0$, respectively.

Region $c$ extends form $x = J_1 = x_{J1}$ to $x = K_0 = x_{K0}$ where $y(x)$ is defined as:

$$y(x) = \alpha v - \beta v^2 + a \tag{B-13}$$

where $v = x - x_{J1}$. In this region, the first and second derivatives of the normalized flux linkage are given by:

$$\frac{dy}{dx} = \frac{dy}{dv} = \alpha - 2\beta v \tag{B-14}$$

At P (see Figure B-2), $x = x_{J1}$, then $\left.\frac{dy}{dx}\right|_{x=x_{J_1}} = \alpha = m_P$ since $v = 0$.

At Q, $x = x_{K0}$, then $v = c$ and $\left.\frac{dy}{dx}\right|_{x=x_{K0}} = \alpha - 2\beta c = m_Q \Rightarrow \beta = \frac{m_P - m_Q}{2c}$.

The next step is to apply the boundary conditions in order to obtain the system equations to solve for the five unknowns $a$, $b$, $h$, $m_P$, and $m_Q$ (graphically shown in Figure B-2).

From Figure B-2, $$a + b + h = 1 \tag{B-15}$$

From (B-7), $$a = \frac{m_P\, j}{2} \tag{B-16}$$

From (B-10), $$b = \frac{2\, m_Q\, k}{\pi} \tag{B-17}$$

From (B-13), $$h = \frac{c\left(m_P + m_Q\right)}{2} \tag{B-18}$$

The ratio between the gradients at $P$ and $Q$ (typically < 1) is the equation that defines the system completely; that is,

$$\mu = m_Q/m_P \tag{B-19}$$

Finally, (B-15) can be rewritten as:

$$m_P = \frac{2}{j + c(1+\mu) + \frac{4k\mu}{\pi}} \tag{B-20}$$

Knowing $J_0$, $J_1$, $K_0$, $K_1$, and $\mu$, the others values required for a complete definition of the normalized gage curve can be obtained by applying (B-15)-(B-20).

In order to adapt the normalized gage curve to a particular SRM topology, FEA simulations or measurements are required. As shown in Figure B-3, the flux linkage is measured/calculated at several rotor positions using two different current levels: $i_1 < i_s$ and $i_2 >> i_s$ where $i_s$ is the current at which the SRM reaches saturation being at the aligned rotor position. These (approximately 20) measurements are used to plot the normalized gage curve and to calculate graphically the coefficients $J_0$, $J_1$, $K_0$, $K_1$, and $\mu$. In addition, the mathematical formulations of the unaligned and aligned flux-linkage curves are derived from the same measurements. Once that the normalized gage-curve mathematical structure has been defined the next step is the modeling of the shape variations of the gage curve because of changes on the phase current level. This is accomplished in the following section.

### B.2.3 Variation of the Gage-Curve Coefficients

These shape changes of the normalized gage curve can be modeled by means of width changes of the different regions (see Figure B-2). At low phase-current levels ($i < is$), the points J and K can be assumed fixed. However, the widths of the region j and k increase with increasing phase-current level. This characteristic of the normalized gage curve can be taken into account if the points J0 and K0 migrate towards $x = 0$ and the points J1 and K1 migrate towards $x = 1$. The rate of variation for each point with respect to the current level is assumed constant. This assumption makes the model more empirical; however, it is considered justifiable because the structure of the gage curve remains simple and able to model the observed properties of the SRM. Thus, the variation of the breakpoints are expressed as follows:

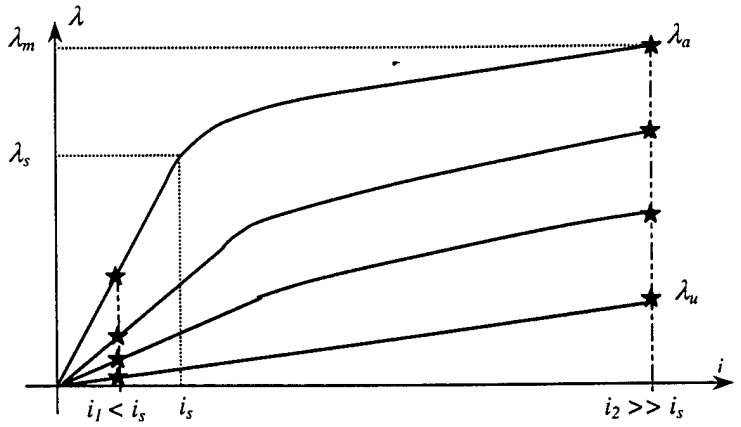


*Figure B-3. Measurements required for the normalized gage-curve formulation.*

$$J_0' = J_0 + W_{J0}\ i \qquad \text{For } i > i_s \qquad \text{(B-21)}$$

$$J_1' = J_1 + W_{J1}\ i \qquad \text{For } i > i_s \qquad \text{(B-22)}$$

$$K_0' = K_0 + W_{K0}\ i \qquad \text{For } i > i_s \qquad \text{(B-23)}$$

$$K_1' = K_1 + W_{K1}\ i \qquad \text{For } i > i_s \qquad \text{(B-24)}$$

where $W_{J0}$, $W_{J1}$, $W_{K0}$, and $W_{K1}$ are the rates of variation. The assumption of the width variation for regions $j$ and $k$ sets the variation of the width for region $c$, which in turn modifies the value of $m_P$ as shown in (B-22) (see Figure B-2). Moreover, the value of $\mu$ also changes from (B-21). The following expression considers this effect:

$$\mu = 1 - \frac{x_{kj}}{c}(1 - \mu_0) \qquad \text{(B-25)}$$

where $x_{kj}$ is the fixed distance between $j$ and $k$, $\mu_0$ is the chosen value of $\mu$ under no saturation conditions, and $c$ is the width of region $c$ under the actual saturation level.

Now that the normalized gage curve has been completely defined, it will be used in the next section to calculate the instantaneous phase current and torque.

### B.2.4 Instantaneous Phase Current and Torque Calculation

The normalized gage curve should be 'de-normalized' by means of mathematical expressions for the aligned and unaligned flux linkages in order to calculate the instantaneous phase current. The following assumptions are made to define these mathematical expressions as illustrated graphically in Figure B-4.

*a)* The unaligned magnetization curve is assumed to be a straight line; consequently,

$$\lambda_u = L_u\, i \tag{B-26}$$

*b)* The aligned magnetization curve is assumed to be a straight line for $i < i_s$ and a parabola for $i > i_s$; consequently,

$$\lambda_{au} = L_{a0}\, i \qquad \text{For } i < i_s \tag{B-27a}$$

$$(\lambda_a - \lambda_{s0})^2 = 4\, a\, (i - i_{s0}) \quad \text{For } i \geq i_s \tag{B-27b}$$

The following constrains are applied to ensure a continuous gradient at $i = i_s$:

$$\lambda(i)\big|_{i=i_s} = \lambda_s \Rightarrow (\lambda_s - \lambda_{s0})^2 = 2\, a\, (i_s - i_{s0}) \Rightarrow i_{s0} = i_s - \frac{a}{L_{a0}^2} \tag{B-28}$$

and,

$$\left.\frac{di}{d\lambda}\right|_{\lambda=\lambda s} = \frac{1}{L_{a0}} \Rightarrow \frac{2(\lambda_s - \lambda_{s0})}{4a} + i_{s0} = \frac{1}{L_{a0}} \Rightarrow \lambda_{s0} = \lambda_s - \frac{2a}{L_{a0}} \tag{B-29}$$

The third equation needed to determine the constant $a$ in (B-27b) is derived from the equation of the parabola evaluated at M (see Figure B-4); this yields

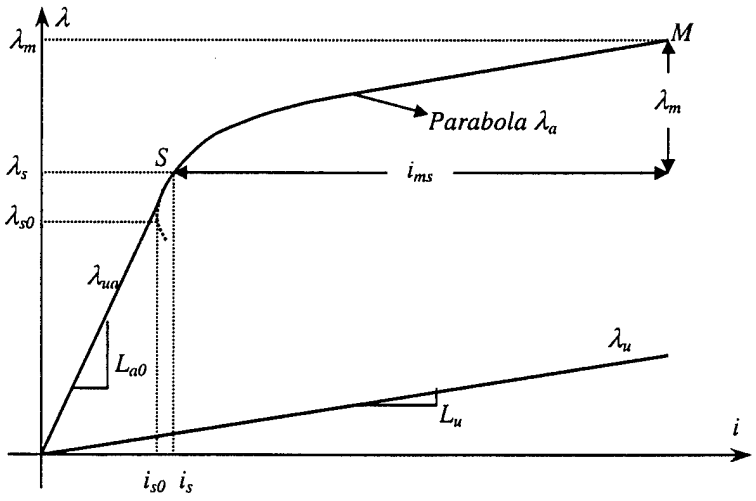


*Figure B-4. Unaligned and aligned magnetization curves.*

$$a = \left.\frac{(\lambda_s - \lambda_{s0})}{4(i_s - i_{s0})}\right|_{\lambda=\lambda_M} = \frac{(\lambda_M - \lambda_{s0})}{4(i_M - i_{s0})} = \frac{\left(\lambda_M - \lambda_s - \frac{2a}{L_{a0}}\right)}{4\left(i_M - i_s - \frac{2a}{L^2_{a0}}\right)} \Rightarrow$$

$$(\lambda_{ms} L_{a0})^2 + 4\,\lambda_{ms} L_{a0}\, a + 4\, a^2 = 4\, i_{ms} L^2_{a0}\, a + 4\, a^2 \Rightarrow$$

$$a = \frac{\lambda^2_{ms}}{4\left[i_{ms} - \frac{\lambda_{ms}}{L_{a0}}\right]} \qquad \text{(B-30)}$$

where, $\lambda_{ms} = \lambda_m + \lambda_s$, and $i_{ms} = i_m - i_s$.

Just one point is needed to calculate the unaligned magnetization curve. Two points, S and M, are required to calculate the aligned magnetization curve, and only one of them, M, requires a non-linear calculation.

Finally, the assumption of a quadratic behavior for the aligned magnetization curve for $i \geq i_s$ implies certain constrains since a second-order polynomial appears to be not accurate enough to model the aligned magnetization curve. However, the loss of accuracy seems to be insignificant when the simulation results are compared with test data [B.4]. Furthermore, the use of a quadratic form will provide small computational-time requirements.

The final step is the derivation of an equation for the instantaneous torque. By expressing the flux linkage as the product of two functions, $\lambda(i,\theta)=f_1(i)f_2(\theta)$, a explicit expression for the instantaneous torque can be derived using $T_e = \frac{\partial W'}{\partial \theta}$ from the integral of coenergy, $W' = \int_0^i \lambda(i,\theta)\,di$. The normalized gage curve allows us to obtain such a flux-linkage expression ($y(x)$) by means of explicit expressions for the unaligned and aligned flux linkages. Since the aligned flux-linkage equation is defined using two different mathematical expressions (one for $i < i_s$ and another one for $i \geq i_s$), the definition of the torque equation will be divided into two regions as follows:

<u>If $i < i_s$</u>

From (B-5) $$\lambda(x) = (1-y(x))\,\lambda_u + y\,\lambda_a$$

From (B-26) and (B-27a)

$$\lambda(x) = [L_u\,(1-y(x)) + y(x)\,L_{a0}]\,i \qquad \text{(B-31)}$$

From (A-2) $W'(\theta,i)=\int_0^i \lambda(\theta,i)\,di$. Therefore,

$$W'=\int_0^i \lambda(x)\,di=\int_0^i [L_u(1-y(x))+y(x)L_{a0}]\,i\,di=[L_u(1-y(x))+y(x)L_{a0}]\frac{i^2}{2} \quad \text{(B-32)}$$

And $T(\theta,i)=\left.\frac{\partial W'}{\partial \theta}\right|_{i=const.}$. Consequently,

$$T_e(\theta,i)=\frac{\partial W'}{\partial \theta}=\frac{\partial W'}{\partial y}\frac{dy}{dx}\frac{dx}{d\theta} \quad \text{(B-33)}$$

where,

From (B-32) $$\frac{\partial W'}{\partial y}=[L_{a0}-L_u]\frac{i^2}{2} \quad \text{(B-34)}$$

From (B-6) $$\frac{dx}{d\theta}=\frac{1}{\theta_a-\theta_u} \quad \text{(B-35)}$$

Finally, depending upon the value of $x$,

$$\frac{dy}{dx}=\begin{cases} 0 & 0\le x<J_0 \\ \frac{m_P}{2}[1-\cos(q*u)] & J_0\le x<J_1 \\ \alpha-2*\beta*v & J_1\le x<K_0 \\ m_Q\cos(r*z) & K_0\le x<K_1 \\ 1 & K_1\le x<1 \end{cases} \quad \text{(B-36)}$$

Consequently,

$$T_e=\left[[L_{a0}-L_u]\frac{i^2}{2}\right]\frac{1}{\theta_a-\theta_u}\frac{dy}{dx} \quad \text{(B-37)}$$

<u>If $i \ge i_s$</u>

From (B-5) $\lambda(x)=(1-y(x))\,\lambda_u+y(x)\,\lambda_a$

From (B-26) and (B-27b)

$$\lambda(x)=(1-y(x))L_u\,i+y(x)\left(2\sqrt{a}\sqrt{i-i_{s0}}+\lambda_{s0}\right) \quad \text{(B-38)}$$

$$W' = \int_0^i \lambda(x)di = \int_0^{is} [(1-y(x))L_u + y(x)L_{a0}]i\,di + \int_{is}^{i} \left[(1-y(x))L_u\, i + y(x)\left(2\sqrt{a}\sqrt{i-i_{s0}} + \lambda_{s0}\right)\right]di =$$

$$L_u \frac{i^2}{2} + y(x)\left[L_{a0}\frac{i_s^{\,2}}{2} - L_u\frac{i^2}{2} + \lambda_{s0}(i-i_s) + \frac{4}{3}\sqrt{a}\left((i-i_s)^{3/2} - (i_s - i_{s0})^{3/2}\right)\right] \quad \text{(B-39)}$$

From (B-33)

$$T_e = \left[L_{a0}\frac{i_s^{\,2}}{2} - L_u\frac{i^2}{2} + \lambda_{s0}(i-i_s) + \frac{4}{3}\sqrt{a}\left((i-i_s)^{3/2} - (i_s - i_{s0})^{3/2}\right)\right]\frac{1}{\theta_a - \theta_u}\frac{dy}{dx} \quad \text{(B-40)}$$

Equations (B-37) and (B-40) are the instantaneous torque equations for phase currents smaller and larger that the saturation current $i_s$, respectively. At this point, all the equations required for the gage-curve simulation technique have been defined. In the next section, a 'step' of the dynamic simulation of a SRM using this technique is presented in order to illustrate how all the defined equations works together.

### B.2.5 One Step of the Simulation Process

In this section, a simulation *step* is solved to clarify the relations among the normalized gage-curve, the instantaneous phase current, the instantaneous torque and the mechanical equations. Note that the equations are solved sequentially as in the simulation program.

Given the following initial conditions:

$i(t_0) = 0$, $\lambda(t_0) = 0$, $\theta(t_0) = \theta_{unaligned}$, $\omega(t_0) = 0$, $V(t_0) = V_{dc}$, $T_L(t_1) = constant$, and $t_0 = 0$

First step $n = 1$:

The time steps of the SRM dynamic simulation are expressed by:

$$t_1 = to + n\,\Delta T = \Delta T, \quad \text{(B-41)}$$

From (B-2) the new value of the flux linkage is calculated based on the previous values of current and rotor position as follows:

$$\lambda(t_1) = \int_{t_0}^{t_1} [\pm V(t) - R\,i(t)]\,dt \cong V_{dc}\,\Delta T \quad \text{(B-42)}$$

The next step is to calculate the new value of current solving (3-31) if the previous current is smaller that the saturation current $i_s$, or solving (3-38) if the previous current is grater that the saturation current $i_s$. Consequently:

If $i(t_1) < i_s$

$$i(t_1) = \frac{\lambda(t_1)}{[L_u(1 - y(x(t_1))) + y(x(t_1))\, L_{a0}]} \qquad \text{(B-43)}$$

with $y(x(t_1)) = \frac{\lambda(t_1) - \lambda_u}{\lambda_a - \lambda_u}$ form (B-5).

If $i(t_1) \geq i_s$, $i(t_1)$ is substituted by an intermediate variable $s = +\sqrt{i - i_{s_0}}$ in (B-38) in order to express (B-38) as a quadratic equation.

$$L_u\,(1\text{-}y(x(t_1)))\, s^2 + 2\,\sqrt{a}\, y(x(t_1))\, s + [y(x(t_1))\, \lambda_{s0} - \lambda(t_1) + (1 - y(x(t_1)))\, i_{s0}\,] = 0 \qquad \text{(B-44)}$$

Solving the quadratic equation in $s$, the new current value is calculated and knowing that $i(t_1) = s^2 + i_{s0}$.

The value for the instantaneous torque $T_e(t_1)$ is calculated applying the present values of rotor position and current to the instantaneous torque equation derived using the normalized gage curve. Consequently,

If $i(t_1) < i_s$

$$T_e(t_1) = \left[ [\, L_{a0} - L_u\, ] \frac{i(t_1)^2}{2} \right] \frac{1}{\theta_a - \theta_u} \frac{dy(x(t_1))}{dx} \qquad \text{(B-45)}$$

where, $\frac{dy(x(t_1))}{dx}$ will depend on the normalized rotor position $x(t_1) = \frac{\theta_1 - \theta_u}{\theta_a - \theta_u}$,

$$\frac{dy(x(t_1))}{dx} = 0 \qquad \text{if } 0 \leq x(t_1) < J_0$$

$$\frac{dy(x(t_1))}{dx} = \frac{m_P}{2}\left[1 - \cos\left((x(t_1) - x_{J0})\frac{\pi}{J_1 - J_0}\right)\right] \qquad \text{if } J_0 \leq x(t_1) < J_1$$

$$\frac{dy(x(t_1))}{dx} = \alpha - 2\beta(x(t_1) - x_{J1}) \qquad \text{if } J_1 \leq x(t_1) < K_0$$

$$\frac{dy(x(t_1))}{dx} = m_Q \cos\left((x(t_1) - x_{K0})\frac{\pi}{2(K_1 - K_0)}\right) \qquad \text{if } K_0 \leq x(t_1) < K_1$$

$$\frac{dy(x(t_1))}{dx} = 1 \qquad \text{if } K_1 \leq x(t_1) < 1$$

If $i(t_1) \geq i_s$

$$T_e(t_1)=\left[L_{a0}\frac{i_s^{\,2}}{2}-L_u\frac{i(t_1)^2}{2}+\lambda_{s0}(i(t_1)-i_s)+\frac{4}{3}\sqrt{a}\left((i(t_1)-i_s)^{3/2}-(i_s-i_{s0})^{3/2}\right)\right]\frac{1}{\theta_a-\theta_u}\frac{dy(x(t_1))}{dx} \quad \text{(B-46)}$$

From (B-3), the speed, $\omega(t_1)$, can be derived as follows:

$$\omega(t_1)=\frac{1}{J_m}\int_{t_0}^{t_1}\left(T_m(t)-T_L(t)\right)dt+\omega_0 \quad \text{(B-47)}$$

From (B-4) the new rotor position, $\theta(t_1)$, can be derived as:

$$\theta(t_1)=\int_{t_0}^{t_1}\omega_1 dt+\theta_0\cong\omega(t_1)\Delta T+\theta_0 \quad \text{(B-48)}$$

At this point, all the *unknown* values $i(t_1)$, $\lambda(t_1)$, $\omega(t_1)$ and $\theta(t_1)$ were calculated. Adding the *known* values $V(t_1)$, $T_L(t_1)$, and $t_2$, the second iteration can be similarly performed.

Figure B-5 shows a block diagram of the gage-curve-based model implementation for only one phase. For the multi-phase case, the phases are considered separately and the total torque is assumed to be the sum of each phase torque (i.e. the principle of superposition by assuming that the phases are independent).

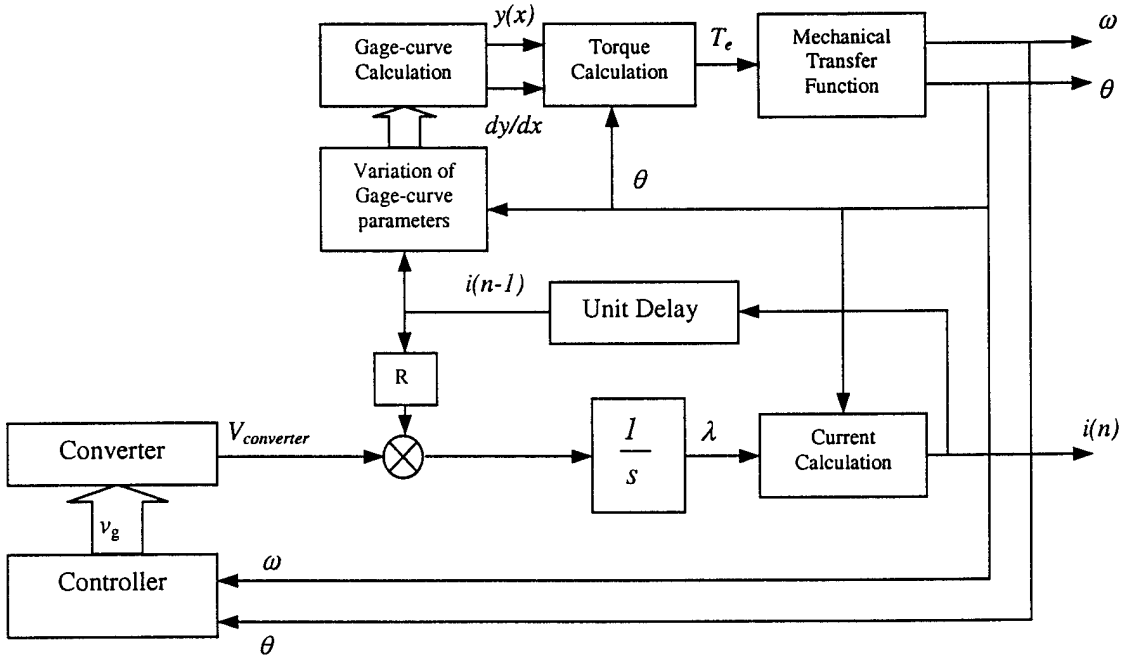


*Figure B-5 Block diagram of the SRM model based on the gave-curve concept.*

Figure B-6 shows the Simulink implementation of a 6/4 SRM drive using the gage-curve concept. Figure B-7 shows the Simulink implementation of one phase.

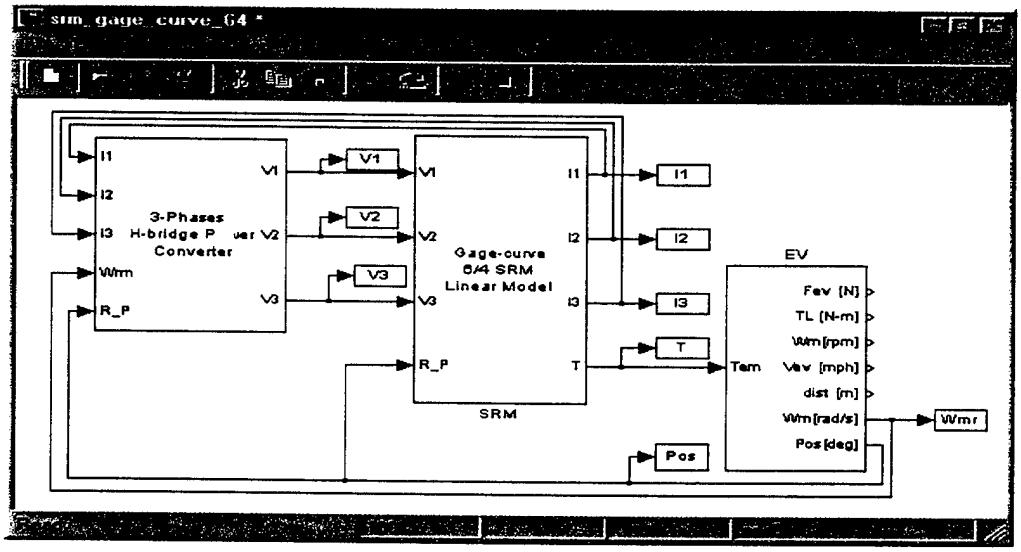


*Figure B-6 Simulink implementation of a 6/4SRM drive using the gage-curve modeling technique.*

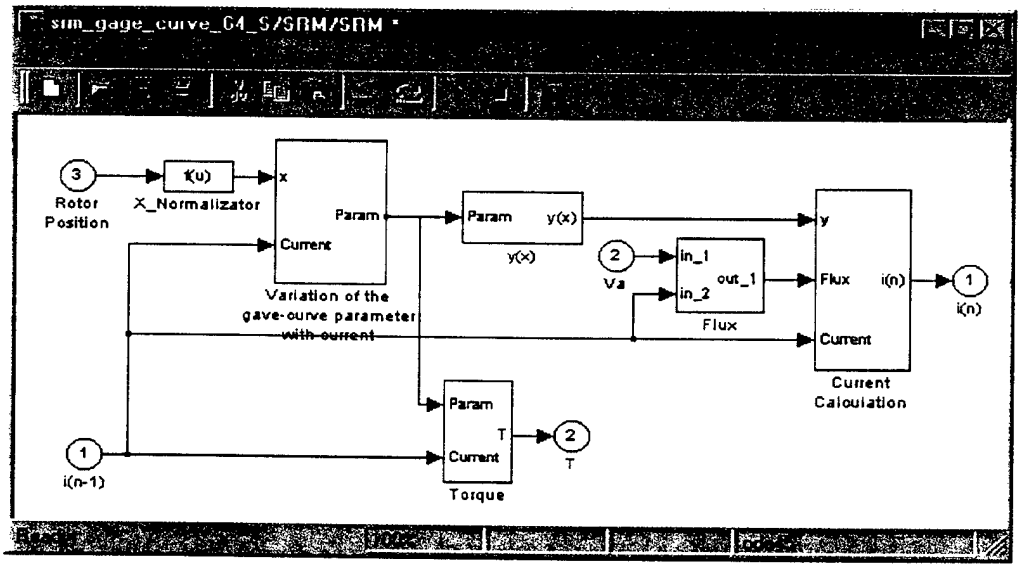


*Figure B-7 Simulink implementation of one phase of the 6/4 SRM using the gage-curve modeling technique.*

The 'look-up table' modeling technique is based on simple mathematical expressions and FEA simulation results. The FEA results are incorporated into the dynamic simulation using look-up tables. The complete descriptions of the phase current vs. the flux linkage with respect to the rotor position as well as the torque vs. the phase current with respect to the rotor position are required from FEA or measurements.

The mathematical expressions used by the 'look-up table' modeling technique are (B-2), (B-3), and (B-4). To obtain the flux linkage, (B-2) is solved through numerical integration at each step of the simulation process as done in the gage-curve technique. However, the required values of the instantaneous phase current $i(t)$ are here calculated using a 'look-up table' which performs a cubic interpolation among the stored data. The flux linkage and the rotor position are required as inputs. Another look-up table is used to calculate the instantaneous torque $T_e(t)$ in which the phase current and rotor position are required as inputs.

Figure B-8 shows the model of a 6/4 SRM drive using the 'look-up table' modeling technique. The multi-phase operation is again modeled as separated single-phase operation (see Figure B-9); it is assumed that the different phases do not have any influence on each other. The total torque is then assumed the sum of the different single-phase torques.

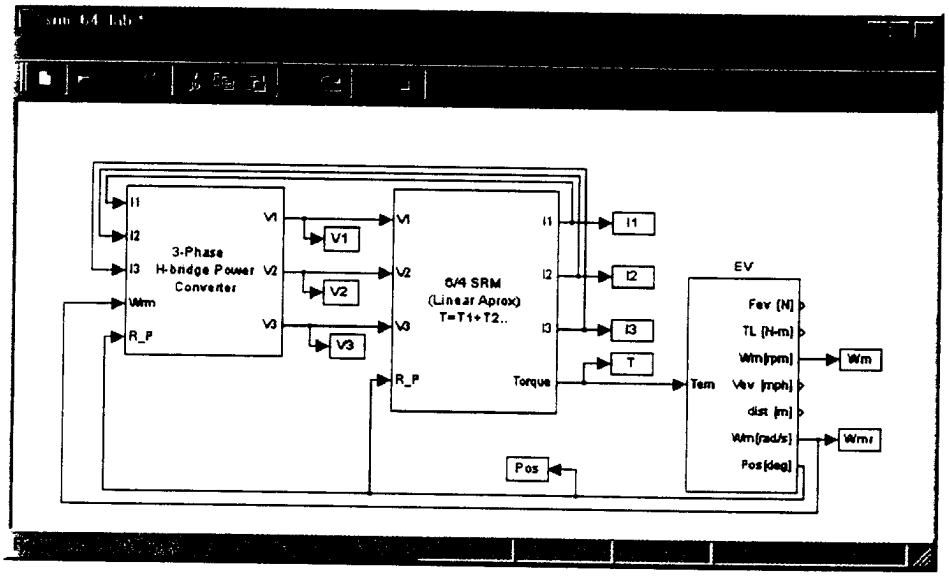


*Figure B-8 Simulink implementation of a 6/4 SRM drive using the 'look-up table' modeling technique.*

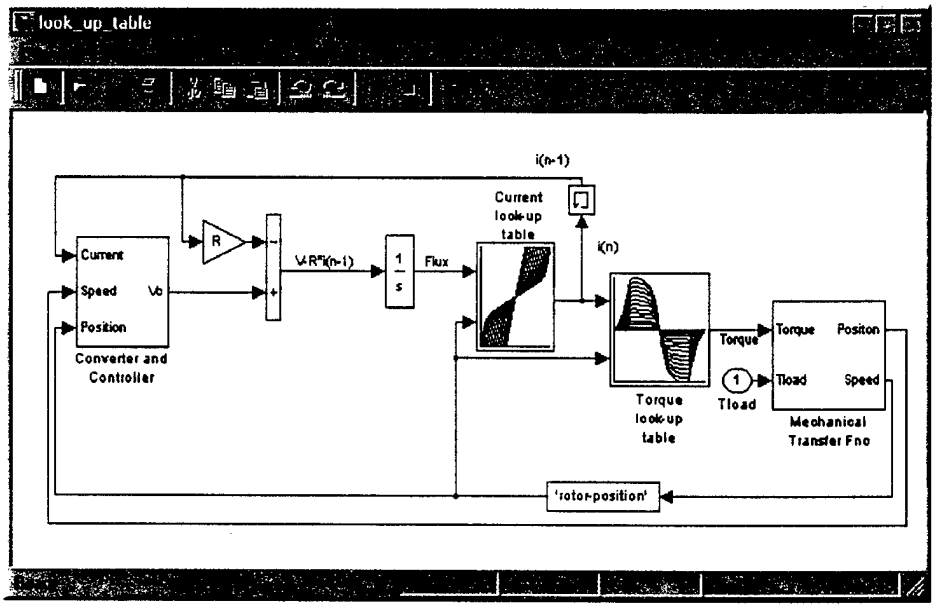


*Figure B-9 Simulink implementation of one phase of the SRM model using the 'look-up table' modeling technique.*

## B.4 Simulations Results

Figure B-10 shows the single-phase static torque prediction by the 'gage-curve' and the 'look-up table' models. The used gage-curve parameters are listed on Table B-1 at the end of this Section. In order to have a closer match between the prediction of the 'gage-curve' and the 'look-up table' models, the following gage-curve parameters are modified: $J_1$ = 0.4 pu and $L_{a0}$ = 170 mH (instead of 0.31 pu and 153.1 mH, respectively). This modified gage-curve-parameter set is used throughout this research. Note that a closer match is achieved by modifying the gage-curve parameters as shown in Figure B-10; however, a difference in 'shape' is present, especially between -45° and -30°. Adjusting the gage-curve parameters cannot eliminate this difference in shape since it is the product of the simplified gage-curve mathematical definition used in this region [B.4].

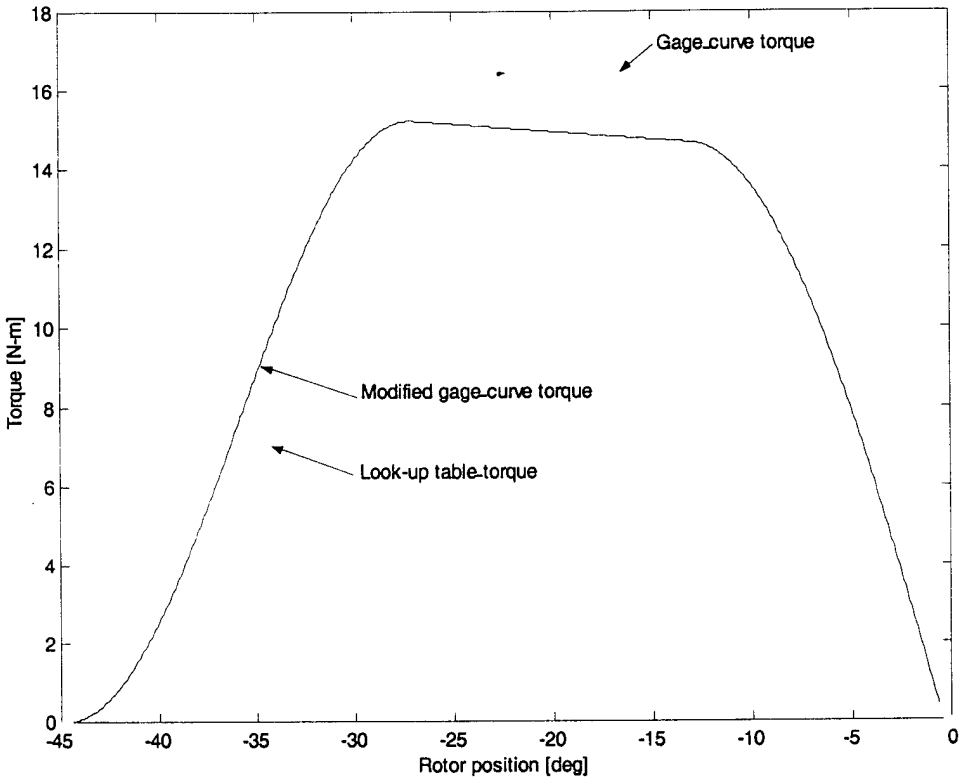


*Figure B-10 Single-phase static torque predicted by the 'gage-curve', 'modified gage-curve' and 'look-up table' models for a phase current of 13A.*

Figure B-11 shows the dynamic multi-phase torque predicted by the 'modified gage-curve' and the 'look-up table' models. Note that the same phase currents are applied to both models; however, there is a difference in the predicted torque. This difference is the product of the difference in the prediction of the single-phase torque shown in Figure B-10 since both models use the superposition principle to obtain the multi-phase torque.

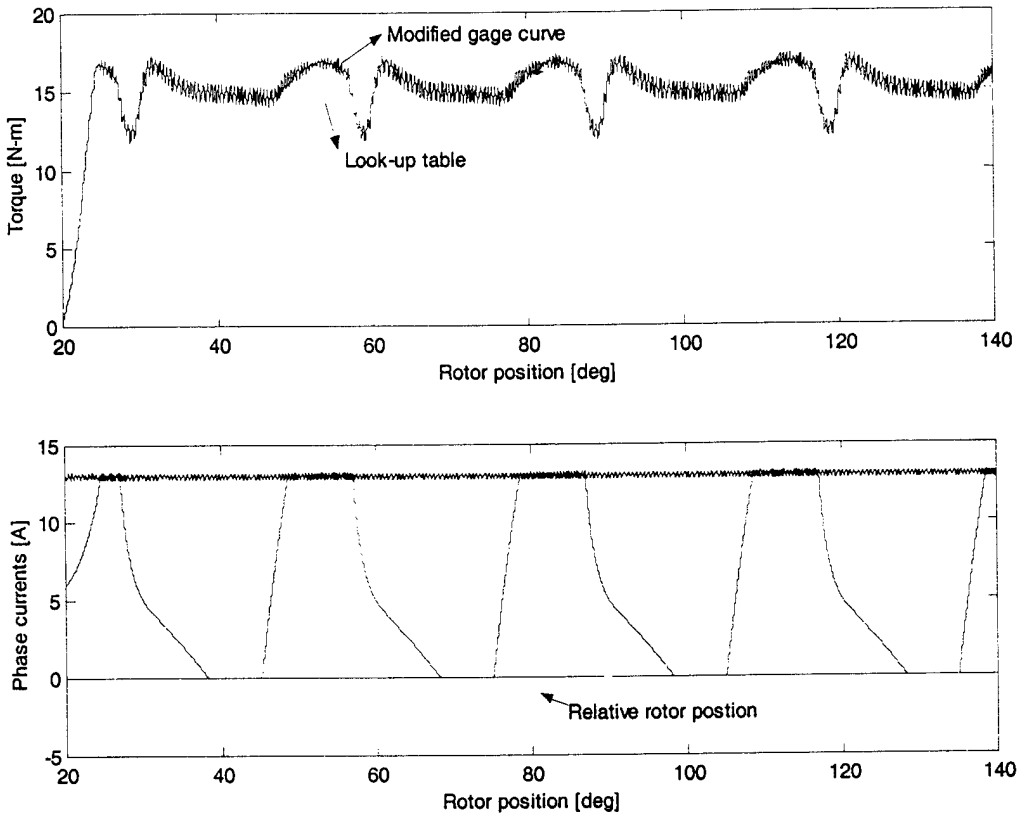


*Figure B-11 Multi-phase dynamic torque predicted by the 'modified gage-curve' and 'look-up table' models for a phase current of 13A.*

Figure B-12 shows the flux linkage and the phase current predicted by the 'modified gage-curve' and 'look-up table' models. Note that the flux linkage predicted by the 'modified gage-curve' model follows closely the theoretical triangular shape of the unsaturated flux linkage (see [B.2] page 59) which is controlled by the mathematical definition of the normalized flux linkage ((B-7), (B-10), and (B-13)).

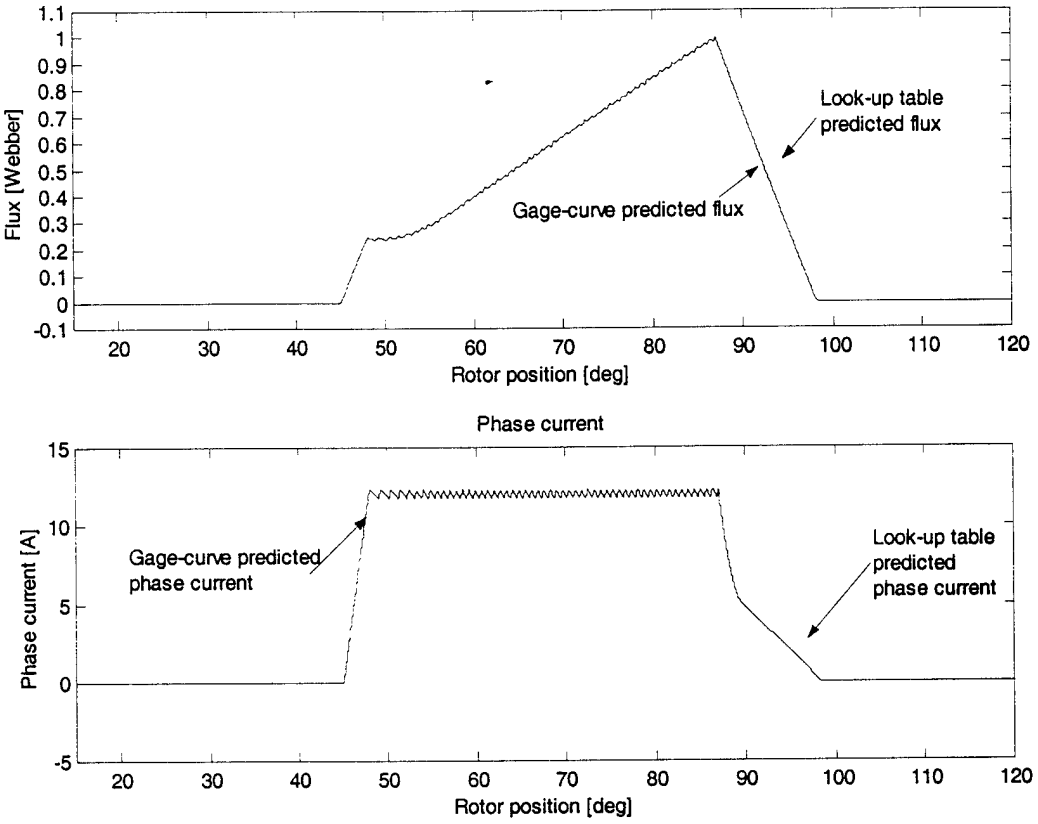


*Figure B-12 Flux linkage and phase current predicted by the 'modified gage-curve' and 'look-up table' models for a phase current of 13A.*

Finally, note that the phase current predicted by the 'look-up table' model decreases slower than the one predicted by the 'gage-curve'. It is because the aligned inductance ($L_{a0}$) was increased in order to get a closer match of the torque waveform.

## B.5 Summary

Although the gage-curve modeling technique requires few data points (typically less that 20) leading to a small computational-time requirement, its implementation and understanding are complex. Moreover, the determination of the used empirical parameters (such as $\mu_0$ , $W_{J0}$, $W_{K0}$) is time consuming and requires previous experience with the modeling technique. In other words, the parameter adjustments require a deep knowledge of the SRM structure because of the empirical nature of the model. Therefore, it is laborious and complex for a person who did not design nor implement the gage-curve model to modify it in order to accomplish the designer's particular needs.

In addition, the advantage of small computational-time requirements is reduced on the Matlab/Simulink implementation because of the large number of equations that has to be implemented (more than 25). To avoid the above-mentioned shortcomings, the 'look-up-table' based SRM modeling technique was developed achieving a simpler to implement and modify modeling technique. In addition, this modeling technique has smaller computational-time requirements. However, it requires a large number of data points, typically 150 data point, (10 samples of the current for 15 different rotor positions).

## B.6 References


[B.1] T. Miller, M. McGilp, "PC-CAD for Switched Reluctance Drive", *Electric Machine and Drive Conference*, London, December 1987, No 2, pp. 360-366.

[B.2] T. Miller, Switched Reluctance Motor and Their Control, Manga Physics Publishing and Clarendon Press - Oxford, 1993.

[B.3] T. Miller, M. McGilp, "Non-Linear Theory of the Switched Reluctance Motor for Rapid Computer-Aided Design", *IEE Proceeding*, Vol. 137, Pt. B, No. 6, November 1990, pp. 337-347.

[B.4] T. Miller, M. Glinka, M. McGilp, C. Cossar, G. Gallegos-Lopez, D. Ionel, M. Olaaru, "Ultra-Fast Model of the Switched Reluctance Motor", *Proceeding of the Industrial Applications Society Annual Meeting*, 1998, pp. 319-326.

Table B-1 Gage-curve parameters of the considered 6/4 SRM.

| Gage-curve parameters | |
|---|---|
| $J_0$ | 0.12 pu |
| $J_1$ | 0.31 pu |
| $K_0$ | 0.96 pu |
| $K_1$ | 1 pu |
| $W_{J0}$ | -0.0075 A/unit |
| $W_{J1}$ | 0.0033 A/unit |
| $W_{K0}$ | -0.0116 A/unit |
| $W_{K1}$ | -0.0011 A/unit |
| $I_s$ | 5 A |
| $I_{s0}$ | 4.8823A |
| $i_{ms}$ | 10 A |
| $\lambda_{ms}$ | 0.2981 Wb |
| $L_{a0}$ | 153.1 mH |
| $L_u$ | 19.9 mH |
| $\lambda_s$ | 0.7656 Wb |
| $\lambda_{s0}$ | 0.7295 Wb |
| $a$ | 0.0028 |
| $\mu_0$ | 0.98 |
| $R$ | 3.2 Ω |

# C MODELING TECHNIQUES FOR MULTI-PHASE-EXCITED SRM

## C.1 Introduction

SRM have been traditionally driven employing single-phase excitation; i.e., only one phase is excited at a time, except during the commutation from one phase to the next one. In recent years, the need for multi-phase modeling techniques increased greatly [C.13-C-15] since it has been proposed that multi-phase excitation can substantially improves the performances of SRM in terms of torque ripple, torque density, efficiency and acoustic noise. Moreover, advanced studies on control strategies and sensorless operation (torque and position) increase further the need for a multi-phase model capable of achieving high accuracy based on a reduced number of measurements [C.16-C.24].

On this Section, the basic equations for the multi-phase operation of the SRM are first introduced. There are two basic differences between the single- and multi-phase excited modeling techniques of a SRM: *a)* the mutual-flux interaction among excited phases, and *b)* the total multi-phase torque. When a single-phase modeling technique is used to predict the multi-phase operation of a SRM, the mutual-flux interaction is usually neglected and the total torque is assumed to be the sum of the individual torques (i.e., superposition principle) developed by each excited phase [C.1-C.12]. An example of this is the use of the 'gage-curve' or 'look-up-table' modeling technique presented in Section B as multi-phase modeling techniques. Next, a new multi-phase modeling technique based on an Analog Neural Network (ANN) and ANSYS-based FEA simulation results is introduced. Next, a 6/4 ANN-based SRM model is implemented using Matlab/Simulink. Finally, a comparison is made with the 'gage-curve' and 'look-up-table' single-phase models implemented in Section B.

## C.2 Multi-Phase Operation of the SRM

The phase voltage equation (A-3) for the single-phase excited SRM can be rewritten for the multi-phase case as follows:

$$V_j = R_j i_j + \frac{d\lambda_j}{dt} \tag{C-1}$$

where $V_j$, $R_j$, $i_j$, and $\lambda_j$ are the applied voltage, resistance, current and flux linkage of the $j$-th phase, respectively.

The flux linkage of the $j$-th phase, $\lambda$, can be expressed as follows:

$$\lambda_j = \lambda_{jj}(i_j,\theta_j) + \sum_{\substack{j\neq k \\ k=1}}^{N_{ph}} \lambda_{jk}(i_k,\theta_k) = \lambda_{jj}(i_j,\theta_j) + \lambda_{jN(i_k,\theta_k)} \qquad \text{(C-2)}$$

where $N_{ph}$ is the number of phases simultaneously excited, $\lambda_{jj}$ is the *self-flux linkage* of the $j$-th phase, $\lambda_j$ is the mutual-flux linkage between the $j$- and $k$-th phases, $\theta_k$ is the relative rotor position of the $k$-th phase with respect to the $j$-th phase and $\lambda_{jN}$ represents the total *mutual-flux linkage* interacting with the $j$-th phase.

The mutual-flux linkage $\lambda_{jN}$ is a nonlinear function of the relative rotor positions and all excited currents. This mutual-flux linkage can be expressed as follows:

$$\lambda_{j_N} = f(i_1,...,i_{N_{ph}},\theta_1,...,\theta_{N_{ph}}) \quad k \neq j \qquad \text{(C-3)}$$

If such a nonlinear function can be determined, the mutual-flux linkage portion can be then subtracted from the (total) flux linkage in order to obtain the self-flux linkage portion. Having determined the self-flux linkage, single-phase-excited SRM modeling techniques can be then used to determine the phase current. In other words, the modeling techniques of Section A modified to account for the mutual-flux linkages can be used as multi-phase-excited SRM modeling techniques. Knowing the phase currents, the total torque can be then determined from a full mapping of the multi-phase torque based on measurements or FEA results.

Here, the 'look-up-table' modeling technique is selected as the modified single-phase-excited SRM modeling technique because the method used to determine (C-3) is based on the coenergy and field energy data points calculated from FEA. Therefore, it is assumed that the flux-linkage characteristic for single-phase excitation required in the 'look-up-table' modeling technique can be easily obtained.

Figure C-1 illustrates the block diagram of the SRM multi-phase-excited model based on the modified 'look-up-table' in order to account for the phase mutual interaction.

This multi-phase model is derived from the single-phase model as follows:

*a)* To calculate the (total) flux linkage of the $j$-th phase, (C-1) is rewritten as follows:

$$\frac{d\lambda_j}{dt} = V_j - R_j i_j \qquad \text{(C-4)}$$

*b)* (C-4) is solved through numerical integration (as in any phase-current technique).

*c)* The mutual-flux linkage is subtracted from the total-flux linkage to obtain the self-flux linkage (see (C-2)).

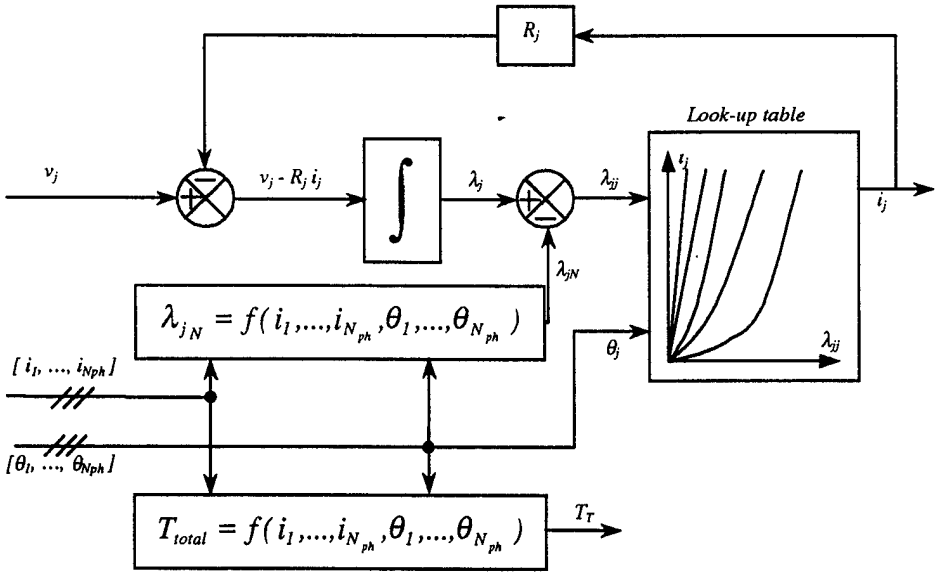


*Figure C-1 Block diagram for the SRM multi-phase model based on the single-phase 'look-up table' modeling technique.*

*d)* The phase current $i_j$ is calculated using cubic-spline interpolation from values stored on a look-up table that has the self-flux linkage $\lambda_{jj}$ and the rotor position $\theta_j$ as inputs in the same fashion as used on the 'look-up-table' modeling technique.

*e)* The total torque is calculated from measurements or FEA results. It is assumed that the full mapping of the total torque is available.

In summary, the two basic differences between the single- and multi-phase modeling techniques have been considered separately by presenting a new approach to account for the mutual fluxes interactions as well as a simplified approach to obtain the multi-phase torque. Hence, the problem of multi-phase modeling of a SRM has been reduced to the derivations/calculations of (C-3) and the multi-phase torque. These issues are further addressed in the next two sections that present a method based on the energy and coenergy of the SRM is presented.

### C.2.1 Mutual-Flux Linkage And Torque Determination

A multi-excited magnetic system (in this case, the SRM under multi-phase excitation) is governed by the following relationship among the flux linkage $\lambda_i$, the phase current $i_i$, the total system coenergy $W_c$, and the total system field energy $W_f$.

$$\sum_{i=1}^{N_{ph}} \lambda_i i_i = W_c + W_f \qquad \text{(C-5)}$$

In order to describe this method, a SRM with two phases simultaneously excited ($N_{ph}$ = 2) is selected; therefore, (C-5) can be expressed as [C.25]:

$$\lambda_1 i_1 + \lambda_2 i_2 = W_c + W_f \tag{C-6}$$

The total-phase fluxes $\lambda_1$ and $\lambda_2$ are divided into *self-flux linkages* ($\lambda_{11}$ and $\lambda_{22}$) and *mutual-flux linkages* ($\lambda_{12}$ and $\lambda_{21}$) as follows:

$$\lambda_1 = \lambda_{11} + \lambda_{12} \tag{C-7}$$

$$\lambda_2 = \lambda_{22} + \lambda_{21} \tag{C-8}$$

Based on these equations, a *mutual interaction function M* can be defined as follows:

$$\lambda_{12} = M(i_1, i_2, \theta)\, i_2 \text{ and } \lambda_{21} = M(i_1, i_2, \theta)\, i_1 \tag{C-9}$$

Then, (C-6) can be rewritten as:

$$\lambda_{11} i_1 + \lambda_{22} i_2 + 2\, M(i_1, i_2, \theta)\, i_1 i_2 = W_c + W_f \tag{C-10}$$

The mutual interaction function $M(i_1, i_2, \theta)$ can be calculated as follows:

$$M(i_1, i_2, \theta) = \frac{W_c + W_f - \lambda_{11} i_1 - \lambda_{22} i_2}{2 i_1 i_2} \tag{C-11}$$

Note that, as was introduced on Section A, the self-flux linkage, the coenergy and the field energy are function of the phase currents and rotor position. Therefore, the mutual interaction function $M$ is a function of phase current $i_1$, phase current $i_2$, and rotor position $\theta$.

Different techniques can be implemented in order to derive the mutual interaction function $M(i_1, i_2, \theta)$. One of the most simple and straightforward techniques is the full mapping of the mutual interaction function using FEA in order to implement a tri-dimensional look-up table (for two-phase excitation). However, it cannot be easily implemented because of the large amount of required FEA-simulations/measurements (see Section A.3). Alternatively, a curve-fitting technique or ANN could be implemented to reduce the amount of information required from FEA-simulations/measurements. Two different techniques were evaluated in this report; namely, Fourier series and ANN.

Fourier series are a well-known curve-fitting technique; however, it requires a large number of FEA-simulation results (600 points or more) for this particular implementation; and its accuracy for certain currents levels and rotor positions is not satisfactory. In addition, Fourier series provides a solution for only the mutual interaction function and not for the total torque.

ANN is a new technique used for this purpose that requires particular knowledge of the SRM system. Traditional ANN structures can be trained using a small number of FEA-simulation results (less than 400 points) while achieving satisfactory accuracy. However, the accuracy of the ANN depends on several variables of the ANN structure (number of layers, number of neurons, number of data points, type of transfer function, training algorithm, etc.). Therefore, several

optimization techniques and generic algorithms can be implemented to improve the ANN accuracy, reduce the number of required data points, reduce the time required for training, simplify the ANN structure, etc.

Up to this point, the presented multi-phase modeling technique is completely general; any SRM topology (i.e., 6/4, 8/6, 10/8, 12/8, etc.) or winding configuration (short, full or fractional pitch) can be implemented. However, the SRM topology and winding configuration modifies the ANN structures and the data points required for training. Therefore, there is not an ANN structures providing the best performance for all SRM configurations; therefore, each configuration should be studied and optimized individually. In the next section, the effects of the SRM topology on the selection of the ANN structures and its training data points is presented by means of an example.

## C.3 Multi-Phase Model Implementation of a 6/4 SRM

In this section, a multi-phase model of a 6/4 SRM is analyzed and implemented using the previously presented multi-phase modeling technique. First, the particular 6/4 SRM topology is analyzed in order to determine the structure and the amount of data required to train the used ANNs.

The 6/4 SRM is essentially designed to operate under single-phase excitation; its stroke angle $\theta_{SR}$ is 30° and its positive torque capability angle $\beta_M$ is 45° (see Section A.2). Therefore, there is a 15° region in which two phases can be simultaneously excited producing positive torque (overlap). As shown in Figure C-2a, phase 1 is the working phase when at pair of rotor poles are at -45° (the unaligned position) with respect to phase 1. At this point, phase 3 (the leading phase) is conducting; therefore, the possible interaction is between the working phase and the leading phase as the working phase approaches 0° (the aligned position) as shown in Figure C-2d. At -30°, the leading phase starts to produce negative torque; therefore, it is usually turned-off; see Figure C-2b. At -15°, phase 3 is completely turned-off (see Figure C-2c) and the other pair of rotor poles is at -45° with respect to phase 2; therefore, phase 2 becomes the working phase and phase 1 the leading phase.

As shown in Figure C-1 two ANNs, one required to predict the mutual-flux interaction ($\lambda_{j_N} = f(i_1,...,i_{N_{ph}},\theta_1,...,\theta_{N_{ph}})$) and the other one required to predict the torque ($T_{total} = f(i_1,...,i_{N_{ph}},\theta_1,...,\theta_{N_{ph}})$), and a look-up table are required to compose each SRM phase.

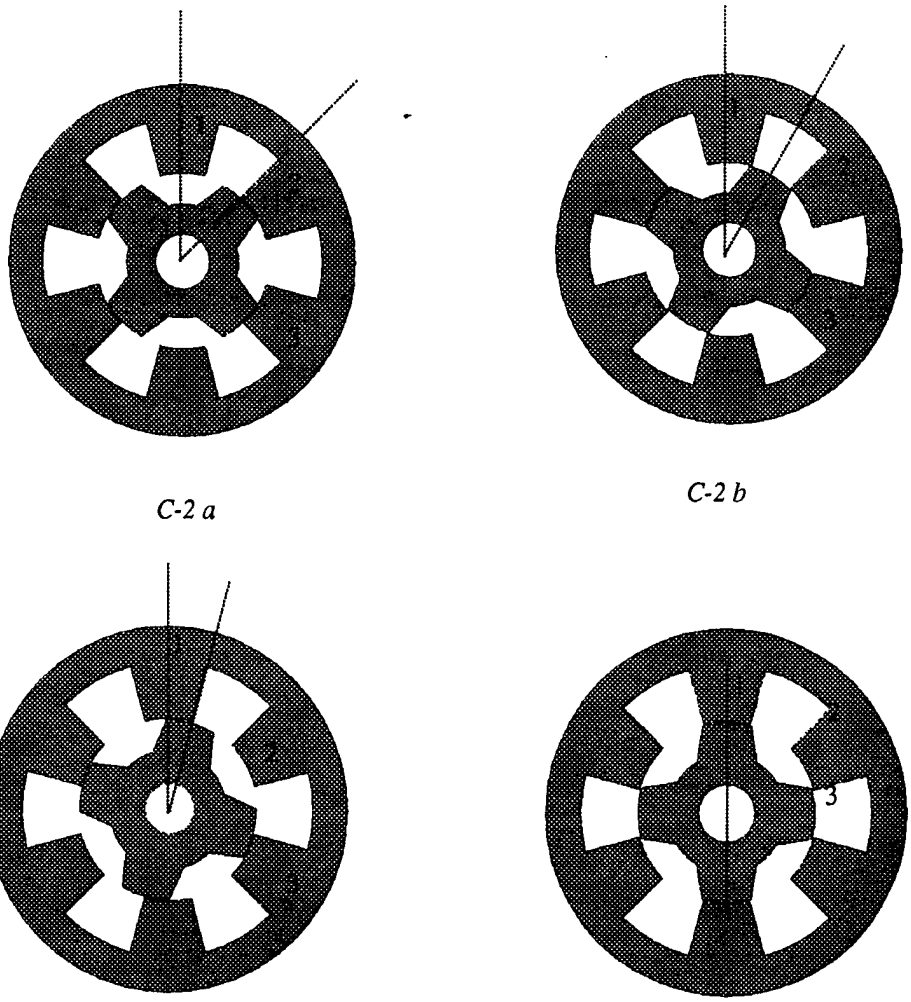

*C-2 a* *C-2 b*

*C-2 c* *C-2 d*

*Figure C-2a 6/4 SRM at -45°. C-2b 6/4 SRM at -30°.*
*C-2c 6/4 SRM at -15°. C-2d 6/4 SRM at 0°.*

In order to establish the ANN structures, a set of training data (in this case calculated by ANSYS-based FEA) is required. In order to obtain such a training data set, the current range is divide into 5 equally-spaced intervals (3A, 6A, 9A, 12A and 15A = $I_{max}$) and the rotor-position range is divide into 11 equally-spaced rotor positions. Therefore, the number of used data points is 5*5*11 = 275. Note that if the same 'density' of data as in the 'look-up table' model were required, the amount of required multi-phase data will be 15*15*16 = 3600 (15 current levels per phase and 16 rotor positions). Finally, the single-phase characteristic used to implement the 'look-

up table' model is incorporated to the training data set since it is already available. Therefore, 240 more points are added for a total of 515.

In order to use just one software package, the handling and training of the ANN is preformed using Matlab. Only two commands in the Matlab ANN toolbox® are used: *newff* and *train*. The *newff* command creates a feed-forward ANN while the *train* command trains the ANN using the back-propagation algorithm. These commands are very simple to use; however, they offer a limited access and control of the training procedure.

Several different combinations of ANN structure, neuron transfer functions and training algorithms were studied for each type of ANN (mutual flux and torque). The selection of the most suitable ANN structures is based on the means square error given by the *train* command. In addition, comparisons are made between a set of testing data composed by 35 data points (obtained in the same way as the training set, but not used to train the ANN) and the predicted results of the ANN. Using this criteria an ANN composed of 3 neurons in the input layer, two hidden layers with 13 and 11 neurons, and a single neuron in the output was selected for the prediction of the mutual function *M*. For the prediction of the torque, the selected ANN was composed of 3 neurons in the input layer, a hidden layer with 13 neurons and a single neuron in the output.

Figure C-3 shows the Simulink implementation of the 6/4 SRM drive using the ANN-based multi-phase technique. Figure C-4 shows the 'inside' of the 6/4 SRM ANN model of Figure C-3. In this Figure, F11, F22 and F33 are the self fluxes of phases 1, 2 and 3, respectively, and FL1, FL2 and FL3 are the mutual fluxes calculated by the ANN allocated inside of the mutual-flux calculator block.

The ANN that predicts the torque is allocated inside of the ANN torque block.

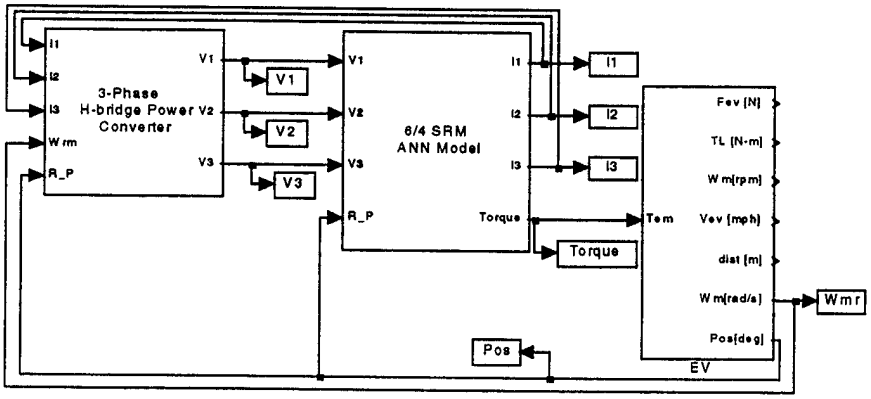


*Figure C-3 Simulink implementation of the 6/4 SRM model using ANNs.*

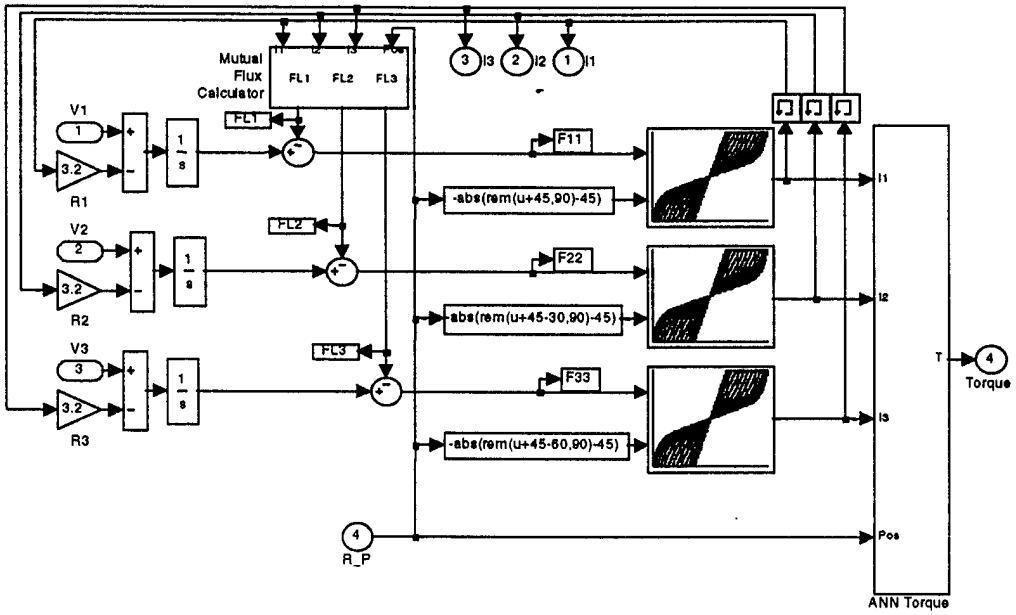


*Figure C-4 'Inside' of the SRM block.*

Figure C-5 shows the total, mutual and self fluxes of the implemented 6/4 SRM operating at a low speed (30 rad/sec). The power converter is set to turn the phase on when the 'participating' rotor-poles pair reaches -45° and turn the phase off when the same rotor-poles pair reaches -3°.

The single-phase modeling techniques, such as the 'look-up table', neglects the effects of mutual interactions among conducting phases predicting only the total flux shown in Figure C-5. This flux, that has the contribution of the leading phase, is used to calculate the working-phase current using the 'look-up table' block. The multi-phase ANN-based technique substracts the portion contributed by the leading phase (calculated by the ANN) from the total flux (see Figure C-4) in order to calculate the flux produced by the working phase. Using this 'modified' flux, which is the self flux in Figure C-5, the working-phase current is calculated using the 'look-up table' block. Note that the total and self fluxes match when the leading-phase current is zero.

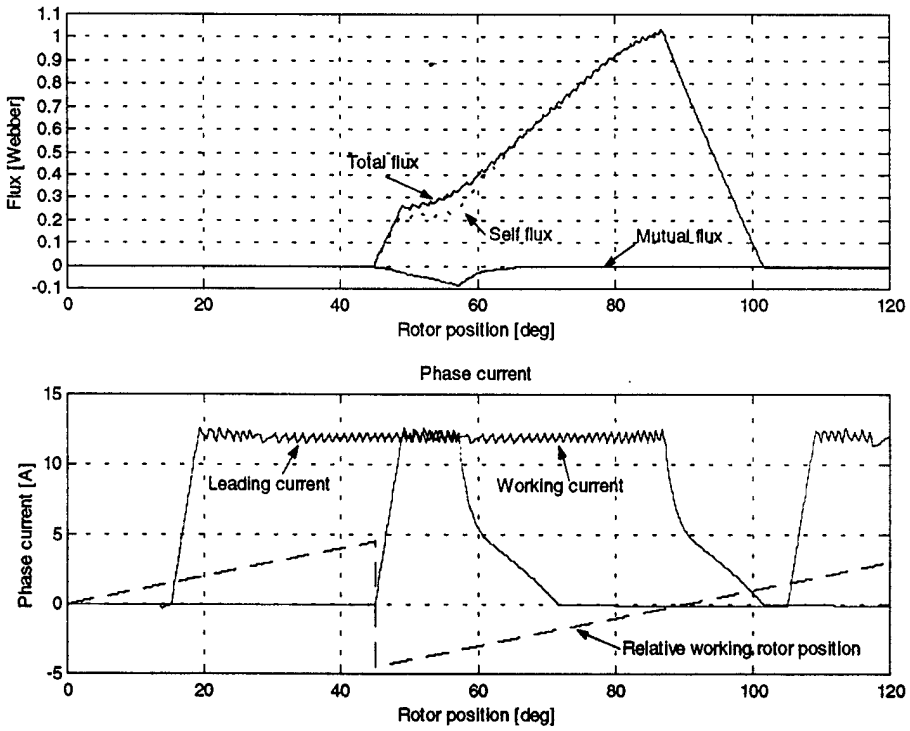


*Figure C-5 Total, mutual and self fluxes of a phase of the 6/4 SRM ANN-based model for low speed operation (30 rad/sec.).*

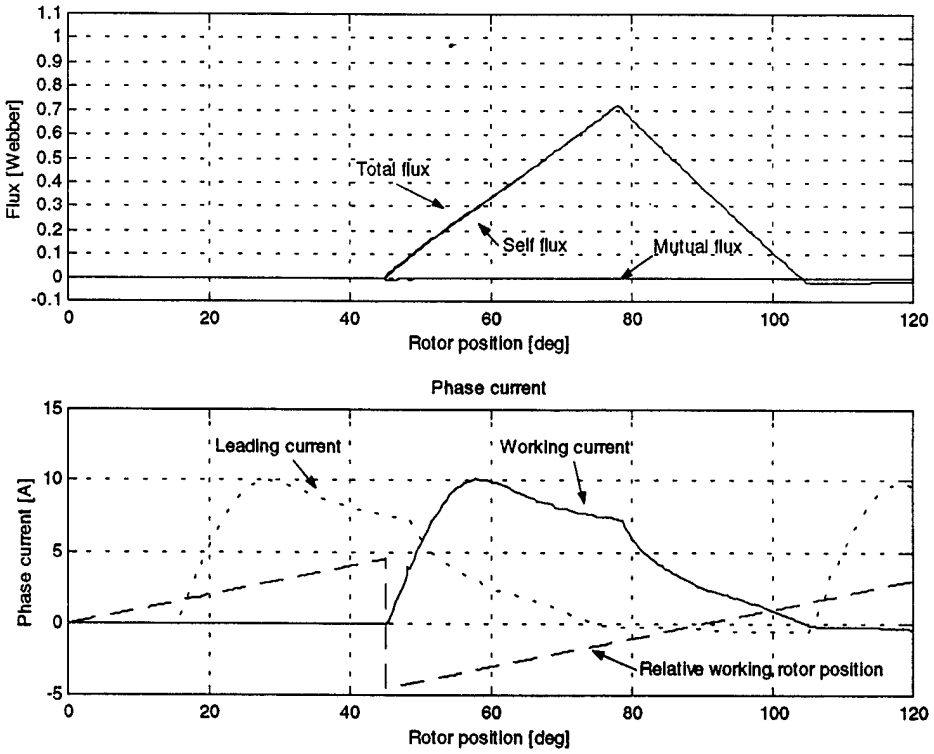


*Figure C-6 Total, mutual and self fluxes of a phase for the 6/4 SRM ANN-based model at high-speed operation (120 rad/sec).*

Figure C-6 shows the total, mutual and self fluxes of the implemented 6/4 SRM operating at a high speed (120 rad/sec). The power converter is set to turn the phase on when 'participating' rotor-poles pair reaches -45° and turn the phase off when the same rotor-pole pair reaches -13°. Note that both the total and self fluxes match as in Figure C-5 when the leading-phase current is zero. It is because at high-speed operation (single-pulse mode) the phase current levels are lower; therefore, the interaction between the leading and working phases is reduced and does not present an important effect.

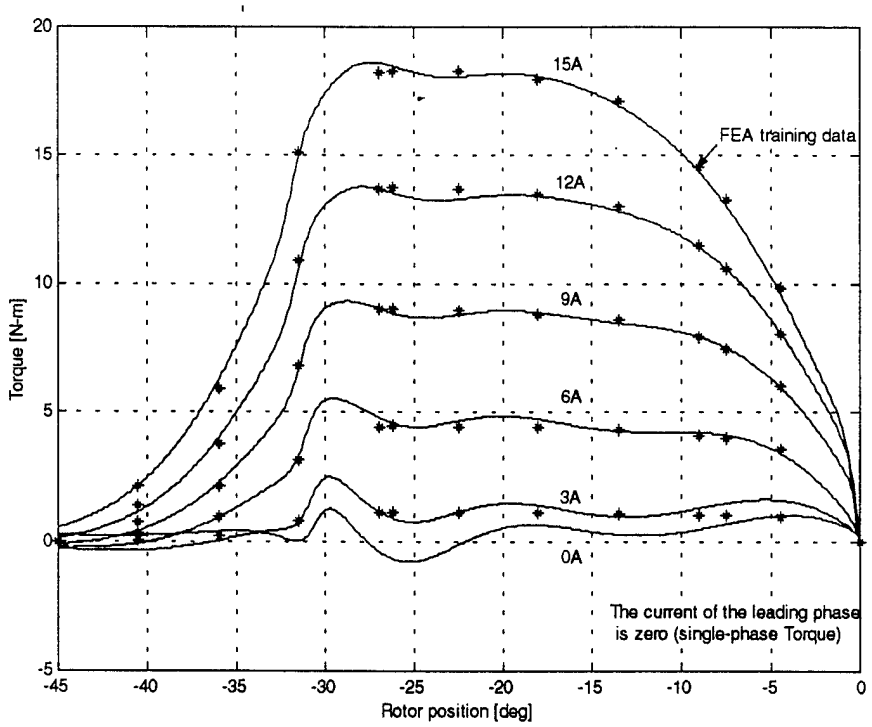


*Figure C-7 ANN prediction of the single-phase static torque and FEA training data.*

Figure C-7 shows the single-phase static torque waveform predicted by the ANN for different current levels in order to illustrate the capability of the ANN-based multi-phase model. In addition, it shows the single-phase portion of the FEA-obtained training data points used to train the ANN. The single-phase torque is obtained from the multi-phase trained ANN by setting the leading current to zero. Note that the differences among the ANN-predicted waveform and the training points are greater at low current levels.

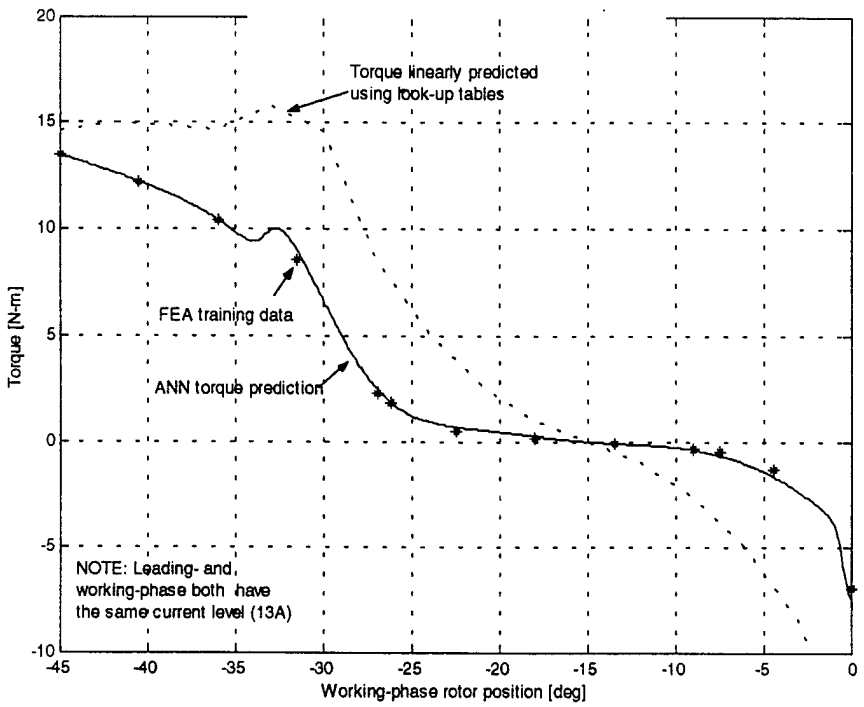


*Figure C-8 ANN prediction of the multi-phase static torque and FEA training data.*

Figure C-8 shows the multi-phase static torque predicted by the ANN-based model, by the 'look-up table' model and the 13A portion of the ANN training data set (obtained by FEA). The leading and working phases carry 13A for the full 45°. However, the difference between the 'look-up table' model and the ANN-based model is smaller at -45° than at around -30°. It is because the flux produced by the working phase at -45° is smaller than at -30° since the reluctance is higher at -45° than at -30°. The main reason for this difference is that the changes on the saturation level of the SRM (because of two phases excited simultaneously) are neglected on the single-phase modeling techniques (such as the 'look-up table' modeling technique).

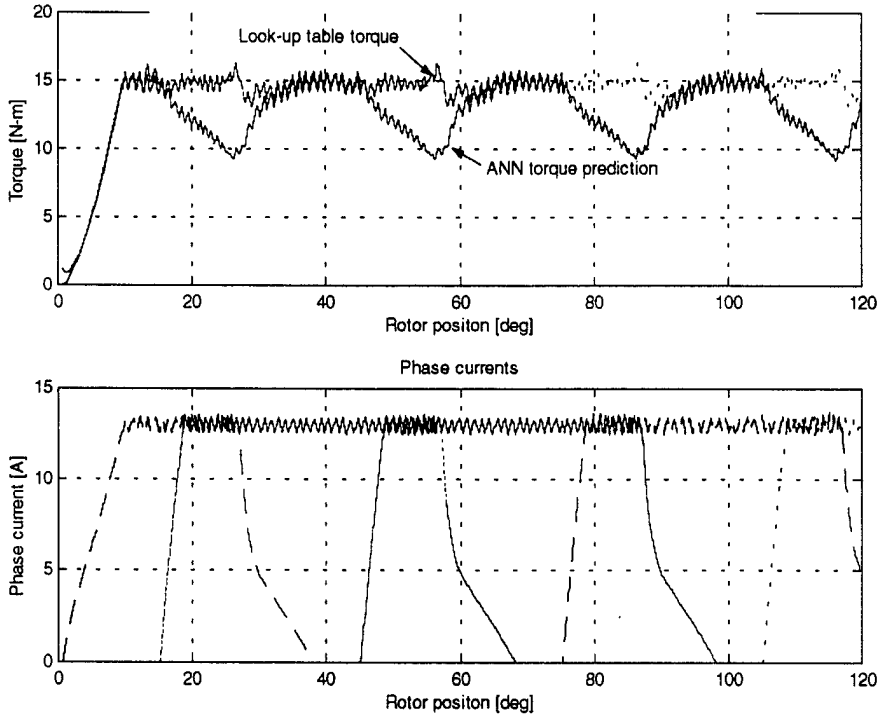


*Figure C-9 ANN and 'look-up table' predictions of the multi-phase dynamic torque.*

Finally, note that the torque is equal to zero at -15° in both techniques because at this rotor position (see Figure C-2c) the amount of attraction produced by the working phase (positive torque) is equal to the amount of repulsion produced by the leading phase (negative torque) since both phases are carrying the same current.

Figure C-9 shows the multi-phase dynamic torque predicted by the ANN-based model and the 'look-up table' model. The dynamic torque predicted by the ANN-based model presents a reduction at certain rotor positions when compared with the dynamic torque predicted by the 'look-up table' model (using the superposition principle). This reduction in torque is produced by the increment on the SRM saturation level when two phases are

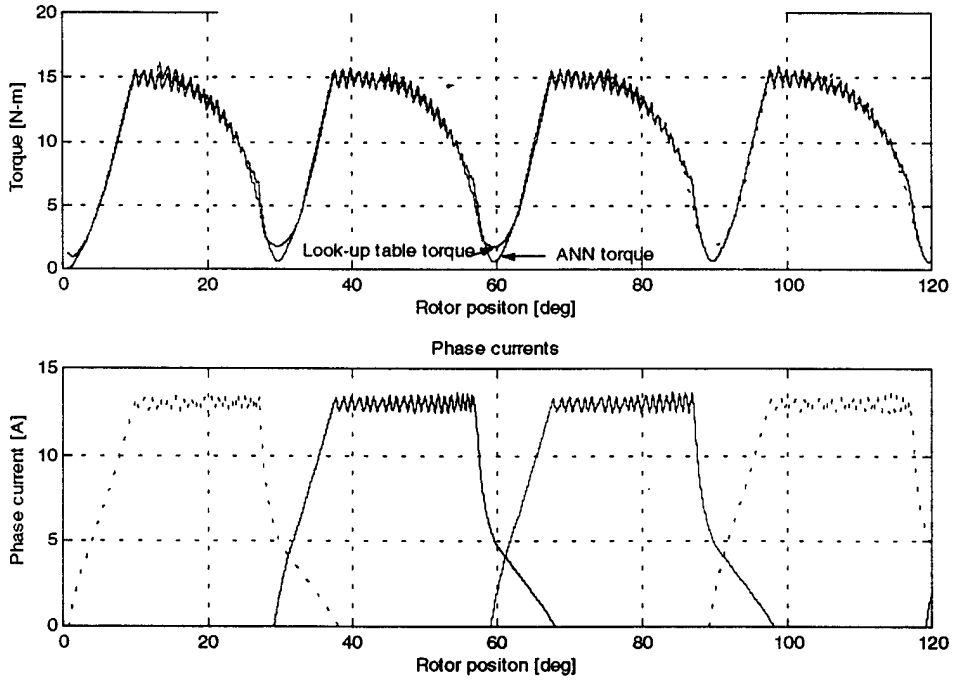


*Figure C-10 ANN and 'look-up table' predictions of the multi-phase dynamic torque.*

excited simultaneously. Note that the torque predicted by single- and multi-phase techniques matches when the SRM operates under single-phase excitation. It will be illustrated later that this torque reduction is also present in the measurements.

Figure C-10 shows the multi-phase dynamic torque predicted by the ANN-based model and the 'look-up table' model. This figure is similar to Figure 4-9. However, the power converter is now set to turn the phase on when the 'participating' rotor-pole pair reaches -33° and turn the phase off when the same rotor-pole pair reaches -13° in order to reduce the overlapping between leading and working phases. Consequently, the torque predicted by the 'look-up table' model (single-phase modeling technique) and the torque predicted using the ANN-based model (multi-phase modeling technique) match closely since the SRM is working essentially under single-phase excitation.

Figure C-11 shows the multi-phase dynamic torque predicted by the ANN-based model and the 'look-up table' model under high-speed operation. Both torque predictions match closely for the same reason that the total and self fluxes match in Figure C-6. At high-speed operation, the current level reached is lower; therefore, the changes in the saturation level of the SRM are reduced.

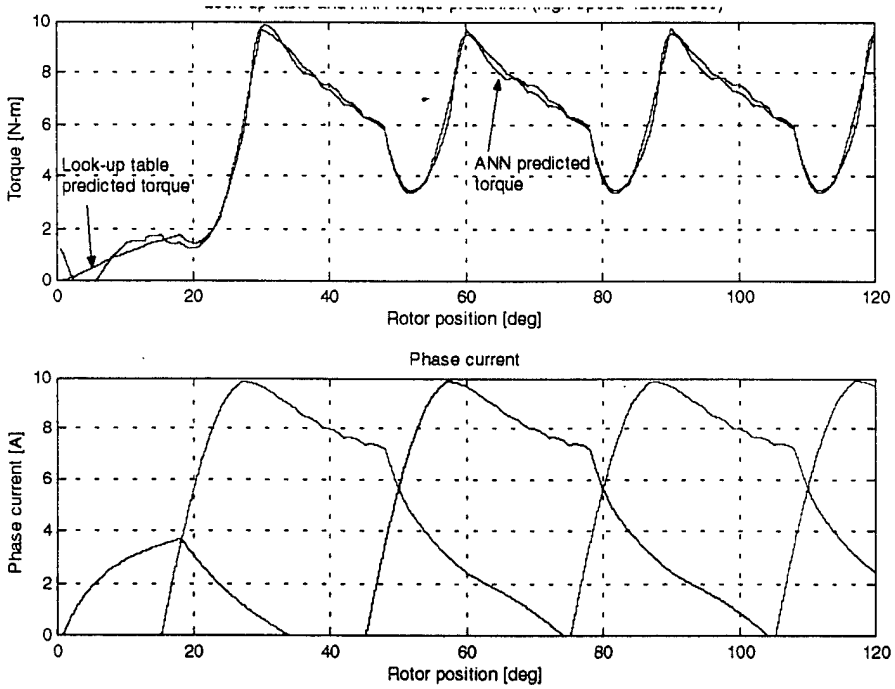


*Figure C-11 ANN and 'look-up table' predictions of the multi-phase dynamic torque for high-speed operation.*

## C.4 The Needs for Measurements

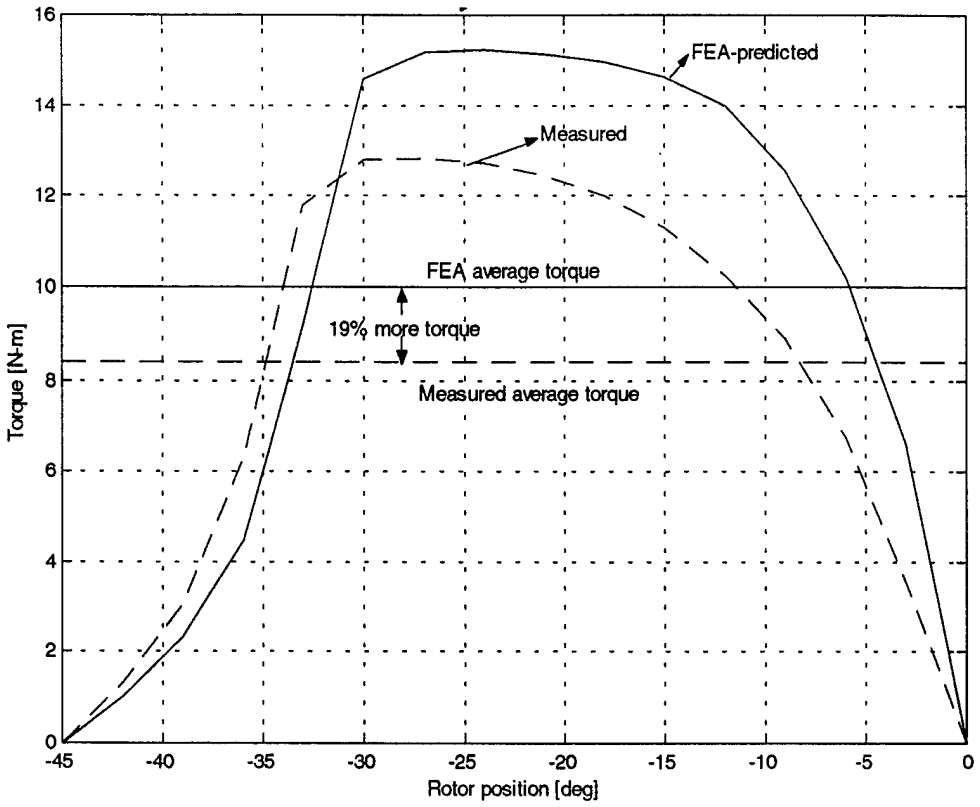


*Figure C-12 Singe-phase static torque comparison between FEA and measurements.*

Figure C-12 shows the comparison between the static torque predicted by FEA and the measured static torque. It has been pointed out that a 2D FEA program such as ANSYS will predict between 15%-20% more torque than the measured torque. Professor Miller mentions in his book *Switched Reluctance Motors and their Control* [C-1] that: "Two-dimensional solvers cannot be expected to give accurate magnetization curves for switched reluctance motors, especially in partially aligned position, because of the significant influence of end effects." In addition, Professor Miller presents a numerical example where the aligned and unaligned inductances computed using 2D and 3D FEA programs are compared with measured aligned and unaligned inductances. The results of this computation/measurement comparison are presented in Table C-1. Note that the difference between the aligned and unaligned inductances using a 2D FEA is 15.3% larger than difference between the measured aligned and unaligned inductances. In addition, the difference between the aligned and unaligned inductances computed using 3D FEA is only 2.8% larger than the difference between the measured aligned and unaligned inductances. The difference between the aligned and unaligned inductances is proportional to the average torque shown in Figure C-12. This large difference between 2D FEA results and measurements strongly suggest that an accurate multi-phase model of the SRM should use 3D FEA results.

However, obtaining the required data points (around 500) using 3D FEA is impractical since it is more complex and time consuming than 2D FEA. Therefore, measurements are required as input data.

*Table C-1 Aligned and unaligned inductances.*

| | Measured | 2D computation | 3D computation |
|---|---|---|---|
| Aligned | 66 mH | 66.5 mH | 68 mH |
| Unaligned | 19.8 mH | 13.2 mH | 20.5 mH |
| Difference | 46.2 mH | 53.3 mH | 47.5 mH |

In order to take the measurements, it is required to setup a test/measurement bench having, in addition to build the SRM, a torque meter, a mechanism that allows blocking the rotor at different positions, two power supplies with current limits and two amperemeters. Once that the test bench had been mounted the measurements of the single- and multi-phase flux-linkage characteristics as well as the torque characteristics are straightforward. Figure C-13 shows a s the general setup of the test/measurements bench. Only torque measurements are presented here; at the writing of this report, this research group is testing a developed method that allows measuring the flux linkage under multi-phase excitation.

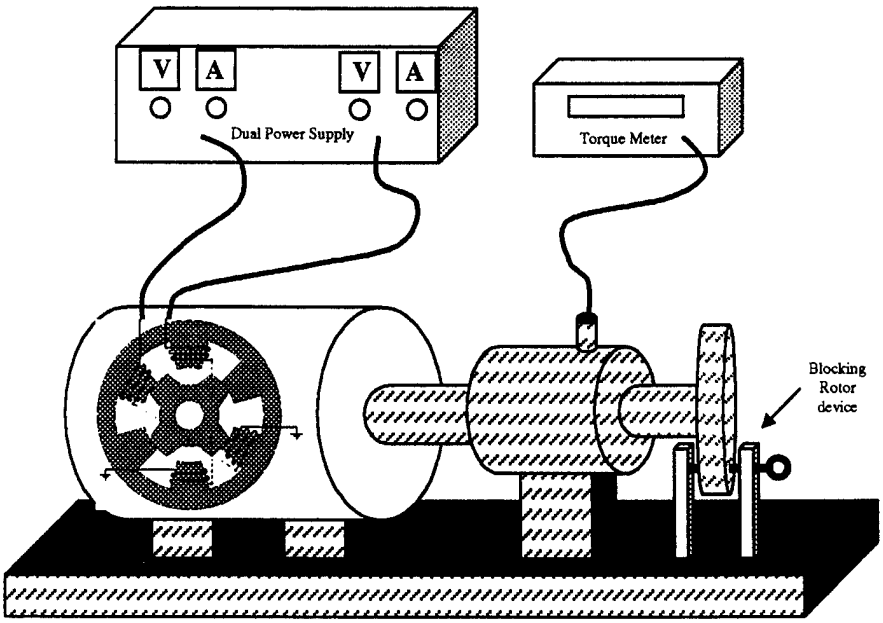


*Figure C-13 General setup of the 6/4 SRM test/measuremnt bench.*

Baldor Motors and Drives (Forth Smith, Arkansas) built the 6/4 SRM used in the test bench.

The equipment used in the test bench were the following:

- 6/4 SRM.
- 6434B Hewlett Packard DC power supply 0-40V, 0-25A.
- 160T60 TCR DC power supply 0-120V, 0-50A.
- 1104-2k Lebow torque sensor, 2000 lb.-in, 9000 rpm.
- 3170 Daytronic strain gage conditioner.
- Two Fluke 73 multimeters.
- Rotor-blocking device capable of blocking the rotor every 3°.

The torque measurements were taken in order to generate a training data set similar to the FEA-based training data set. Therefore, the same phase-current levels were selected (0A, 3A, 6A, 9A, 12A and 15A). However, the measured rotor positions were every 6° instead of 4.5° (0°, 3°, 6°, 12°, 18°, 24°, 30°, 36°, 42° and 45°); the total number of measurements was 6*6*10 = 360. Note that the rotor-blocking device has the capability of only blocking the rotor every 3° or multiple of 3°. Finally, the single-phase torque characteristic was taken every 3° in order to have a better resolution for plotting purposes; however, it was not incorporated into the measured training data set.

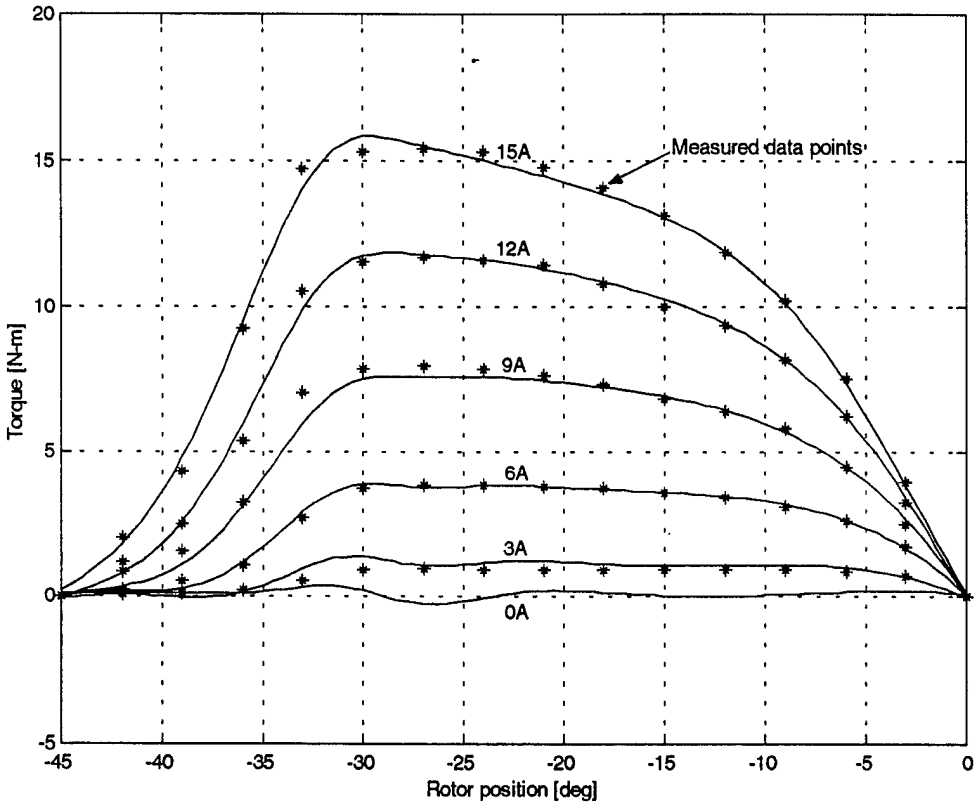


*Figure C-14 ANN prediction of the single-phase static torque and the measured training data.*

Figure C-14 shows the single-phase static torque waveforms for different current levels predicted by the ANN trained with the measured training data set. In addition, it shows the single-phase portion of the measurements used to train such an ANN. The single-phase torque is obtained from the multi-phase trained ANN setting the leading-phase current to zero. Note that, as in Figure C-7, the differences among the ANN prediction and the training points are greater at low current levels.

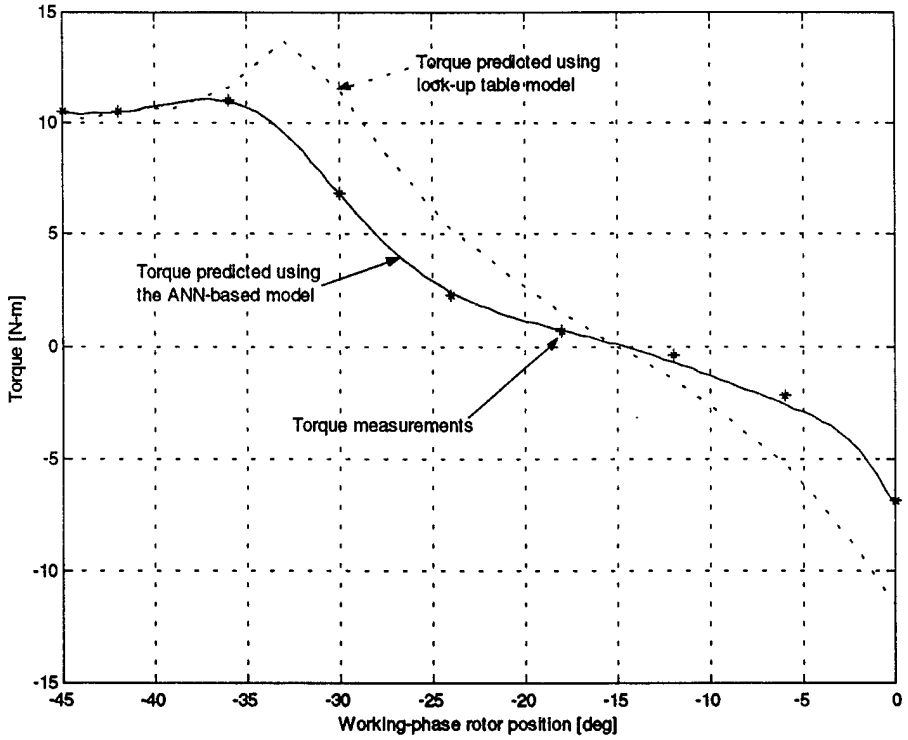


*Figure C-15 ANN prediction of the multi-phase static torque and the measured training data.*

Figure C-15 shows the multi-phase static torque predicted by the ANN-based model and by the 'look-up table' model (by applying superposition principle). Note that, as in Figure C-8, the difference between the 'look-up table' model and the ANN-based model is smaller around -45° (unaligned position) than at -30°. In addition, the torque predicted by the two techniques is zero at -15°. Here, the same explanation presented in Figure C-8 applies.

Figure C-16 shows the multi-phase dynamic torque predicted by the ANN-based model and the 'look-up table' model. Note that, as in Figure C-9, the dynamic torque predicted by the ANN-based model presents a reduction at certain rotor positions compared with the dynamic torque predicted by the 'look-up table' model.

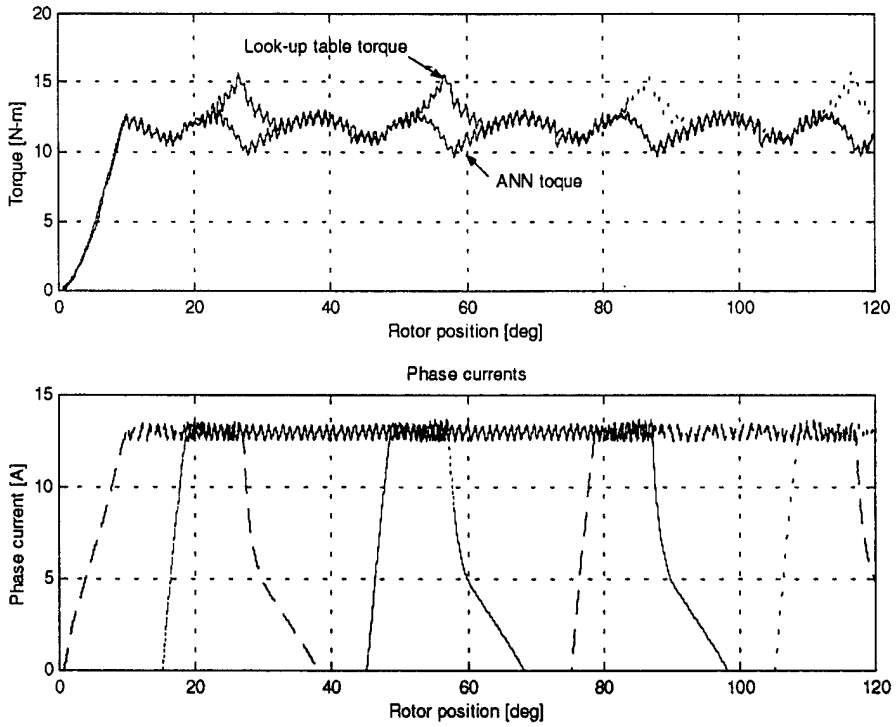


*Figure C-16 ANN and 'look-up table' predictions of the multi-phase dynamic torque.*

In addition, note that there is a change in shape of the torque predicted by the 'look-up table' model on Figure C-15 compared with the torque predicted by the 'look-up table' model on Figure C-9. The reduction of torque predicted by the ANN-based model is produced, as explained on Figure C-8, by an increase in the saturation level of the SRM when two phases conduct simultaneously. The change in shape is produced by the difference between the single-phase static torque predicted by FEA and the single-phase static torque measured (see Figure C-12). The single-phase static torque measured is not only smaller in magnitude but is also 'shifted' about 2°. Since the torque produced by the leading and working phases is added in the 'look-up table' model, this 'shift' produces a peak in the 'look-up table' predicted torque of Figure C-15.

## C.5 Summary

This Section firstly introduced the difference between the SRM single-phase model used to represent a multi-phase operation using the superposition principle and a truly SRM multi-phase model. Next, it presented the basic equations describing the operation of the SRM under multi-phase excitation. Next, it developed a new method based on FEA that accounts for the mutual interaction among conducting phases. This method accounts for the changes on the fluxes of the SRM as well as the torque when exciting a second phase. Next, the developed method was implemented using two ANN. Simulation results (using a single-phase model -the 'look-up table'

model- and a multi-phase model -the ANN-based model-) were compared with measurements. The need for accurate training data was shown based on those comparisons. Finally, torque measurements were taken in order to generate an accurate training data set. Using this measured data set, a new set of plots was made comparing the single-phase model and the multi-phase model. The results of those comparisons were similar to the previously present results; therefore, the capabilities of the new ANN-based multi-phase modeling technique presented in this report to model the behavior of the SRM under multi-phase operation were validated.

## C.6 References


[C.1] T. Miller, Switched Reluctance Motor and Their Control, Manga Physics Publishing and Clarendon Press - Oxford, 1993.

[C.2] Pickup, Tipping, "Method of Predicting the Dynamic Response of a Variable Reluctance Stepping Motor", *IEE Proceeding*, Vol. 120, No. 7, 1973, pp. 757-765.

[C.3] J.V. Byrne, J.B. O'Dwyer, "Saturable Variable Reluctance Machine Simulation Using Exponential Functions", *Proceeding of the International Conference on Stepping Motors and Systems*, University of Leeds, UK, July 1976, pp. 11-16.

[C.4] D.A. Torrey, J.H. Lang, "Modeling a Non-Linear Variable-Reluctance Motor Drive", *IEE Proceeding*, Vol. 137, Pt. B, No. 5, September 1990, pp. 312-326.

[C.5] D.A. Torrey, X-M Niu, E.J. Unkauf, "Analytical Modeling of Variable-Reluctance Machine Magnetization Characteristics", *IEE Proceeding on Electronic Power applications*, Vol. 142, No. 1, January 1995, pp. 14-22.

[C.6] M. Stehpenson, J. Corda, "Computation of Torque and Current in Doubly-Salient Reluctance Motors From Non-Linear Magnetization Data", *IEE Proceeding*, Vol. 126, May 1979.

[C.7] T. Miller, M. McGilp, "PC-CAD for Switched Reluctance Drive", *Electric Machine and Drive Conference*, London, December 1987, No. 282, pp. 360-366.

[C.8] T. Miller, M. McGilp, "Non-Linear Theory of the Switched Reluctance Motor for Rapid Computer-Aided Design", *IEE Proceeding*, Vol. 137, Pt. B, No. 6, November 1990, pp. 337-347.

[C.9] T. Miller, M. Glinka, M. McGilp, C. Cossar, G. Gallegos-Lopez, D. Ionel, M. Olaaru, "Ultra-Fast Model of the Switched Reluctance Motor", *Proceeding of the Industrial Applications Society Annual Meeting*, 1998, pp. 319-326.

[C.10] D.A. Torrey, "An Experimentally Verified Variable-Reluctance Machine Model Implemented in the Saber™ Circuit Simulator ", *Electric Machines and Power Systems*, Vol. 24, No 2, 1996, Taylor & Francis Ltd., pp. 199-209.

[C.11] G. Franceschini, S. Pinari, M. Rinaldi, C. Tassoni "Spice-Assisted Simulation of Controlled Electrical Drives: An Application to Switched Reluctance Drive", *IEEE Transactions on Industry Applications*, Vol. 27, No. 6, November-December 1991, pp. 1103-1110.

[C.12] J. Mahadavi, G Sureseh, B. Fahimi, M. Ehsani, "Dynamic Modeling of Non-Linear SRM Drive With PSPICE", *IEEE Transactions on Industry Applications Society Annual Meeting*, New Orleans, Louisiana, October 5-9, 1997, pp. 661-667.

[C.13] A. Michaelides, C. Pollock, "Modeling and Design of Switched Reluctance Motors with Two Phases Simultaneously Excited", *IEE Proceeding on Electronic Power applications*, Vol. 143, No. 5, September 1996, pp. 361-370.

[C.14] J. Moon, S. Oh, J. Ahn, Y. Hwang, "Switched Reluctance Motors with 2-Phase Excitation", *IEEE Industry Applications Society Annual Meeting*, October 12-15, 1998, pp. 547-552.

[C.15] J. Moon, S. Oh, J. Ahn, Y. Hwang, "A Switched Reluctance Motor Model with Mutual Coupling and Multi-phase Excitation", *IEEE Transactions on Magnetics*, Vol. 27 No. 6, Part 2, November 1991, pp. 5423-5425.

[C.16] M. Preston, J. Lyons, "Torque Estimation in Switched Reluctance Motor Drive Using Artificial Neural Networks", *IECON Proceedings, Industrial Electronics Conference*, Vol. 1, November 9-14, 1997, pp. 21-26.

[C.17] N. Inanc, A. Derdiyok, V. Ozbulur, "Torque Ripple Minimization of a Switched Reluctance Motor Including Mutual Inductances Via Sliding Mode Control Technique", *IEEE International Symposium on Industrial Electronics*, Vol. 3, July 7-11, 1997, pp. 1024-1028.

[C.18] A. Cheok, N. Ertugrul, "High Robustness and Reliability of a Fuzzy Logic Based Angle Estimation Algorithm for Practical Switched Reluctance Motor Drives", *IEEE Annual Power Electronics Specialists Conference*, Vol. 2, May 18-21, 1998, pp. 1302-1308.

[C.19] R. Kavanagh, J. Murphy, M. Egan, "Torque Ripple Minimization in Switched Reluctance Drives Using Self-Learning Techniques", *IEEE Annual Power Electronics Specialists Conference*, Vol. 2, May 18-21, 1998, pp. 1302-1308.

[C.20] Y. Zhan, C. Chan, K. Chau, "A Novel Position and Velocity Observer for Robust Control of Switched Reluctance Motors", *EEE Annual Power Electronics Specialists Conference* Vol. 2, May 18-21, 1998, pp. 1315-1321.

[C.21] Y. Tang, "Improved Control of Switched Reluctance Motor Using Neural Networks and Fuzzy Logic", *Intelligent Engineering Systems Through Artificial Neural Networks*, Vol. 8, November 1-4, 1998, pp. 555-560.

[C.22] D. Panda, V. Ramanarayanan, "Effects of Mutual Inductance on Steady-State Performance and Position Estimation of Switched Reluctance Motor Drive", *IEEE Industry Applications Society Annual Meeting*, October 3-7, 1999, pp. 2227-2234.

[C.23] J. Garside, R. Brown, A. Arkadan, "Switched Reluctance Motor Control with Artificial Neural Networks", *IEEE International Electric Machines and Drive Conference*, Milwaukee, Wisconsin, May 18-21, 1997, pp. TB1-2.1-2.3.

[C.24] L. Belfore, A. Arkadan, "Neurogenetic Models for the Characterization of Fault Tolerant Switched Reluctance Motors ", *IEEE International Electric Machines and Drive Conference*, Milwaukee, Wisconsin, May 18-21, 1997, pp. TB1-8.1-8.3.

[C.25] P. Krause, Analysis of Electric Machinery, McGraw Hill Book Company, 1986.

# REPORT DOCUMENTATION PAGE

*Form Approved*
*OMB No. 0704-0188*



| 1. AGENCY USE ONLY *(Leave blank)* | 2. REPORT DATE | 3. REPORT TYPE AND DATES COVERED |
|---|---|---|
| | June 2000 | Annual Report (Pt. 1), 5/1/99 - 5/30/00 |

**4. TITLE AND SUBTITLE**
Second Annual Report - Part 1 (AR2.1)
Modeling Switched Reluctance Motors Under Multi-Phase Excitation

**5. FUNDING NUMBERS**
G 00014-98-1-0617
PR 98PRO5665-00

**6. AUTHOR(S)**
Roberto M. Schupbach, Shyam S. Ramamurthy
Juan Carlos Balda

**7. PERFORMING ORGANIZATION NAMES(S) AND ADDRESS(ES)**
University of Arkansas, Office of Research and Sponsored Programs, 120 Ozark Hall, Fayetteville, AR 72701

**8. PERFORMING ORGANIZATION REPORT NUMBER**
AR2.1

**9. SPONSORING / MONITORING AGENCY NAMES(S) AND ADDRESS(ES)**
Office of Naval Research
ONR 242
Ballston Centre Tower One, 800 North Quincy Street
Arlington, VA 22217-5660

**10. SPONSORING / MONITORING AGENCY REPORT NUMBER**

**11. SUPPLEMENTARY NOTES**

**a. DISTRIBUTION / AVAILABILITY STATEMENT**
APPROVED FOR PUBLIC RELEASE

**12. DISTRIBUTION CODE**

**13. ABSTRACT** ***(Maximum 200 words)***

Part 1 of 3 of the Second Annual Report covers "modeling" activities performed under task (b) - "Design of the SRM" of this ONR Grant. This Part 1 has been divided into three sections. Section A evaluates different modeling techniques for Switched Reluctance Motors (SRM) operating under single-phase excitation. Section B analyzes two specific techniques for single-phase excitation; namely, the gage curve and 'look-up-table' modeling techniques. Finally, Section C addresses two specific techniques for multi-phase excitation of SRM; one technique is based on the 'look-up-table' used for single-phase excitation, and the other implements an Artificial Neural Network to predict the flux linkage and electromagnetic torque.

**14. SUBJECT TERMS**
Annual report, main activities

**15. NUMBER OF PAGES**
67

**16. PRICE CODE**

| 17. SECURITY CLASSIFICATION OF REPORT | 18. SECURITY CLASSIFICATION OF THIS PAGE | 19. SECURITY CLASSIFICATION OF ABSTRACT | 20. LIMITATION OF ABSTRACT |
|---|---|---|---|
| UNCLASSIFIED | UNCLASSIFIED | UNCLASSIFIED | UL |